Final Report: Characterization of Canister Mockup Weld Residual Stresses

Fuel Cycle Research & Development

Prepared for
U.S. Department of Energy
Used Fuel Disposition Program

D.G. Enos and C.R. Bryan
Sandia National Laboratories

November 22, 2016

FCRD-UFD-2016-000064
SAND2016-12375 R

Sandia National Laboratories is a multi-mission laboratory managed and operated by Sandia Corporation, a wholly owned subsidiary of Lockheed Martin Corporation, for the U.S. Department of Energy's National Nuclear Security Administration under contract DE-AC04-94AL85000.

SUMMARY

Stress corrosion cracking (SCC) of interim storage containers has been indicated as a high priority data gap by the Department of Energy (DOE) (Hanson et al., 2012), the Electric Power Research Institute (EPRI, 2011), the Nuclear Waste Technical Review Board (NWTRB, 2010a), and the Nuclear Regulatory Commission (NRC, 2012a, 2012b). Uncertainties exist in terms of the environmental conditions that prevail on the surface of the storage containers, the stress state within the container walls associated both with weldments as well as within the base metal itself, and the electrochemical properties of the storage containers themselves. The goal of the work described in this document is to determine the stress states that exists at various locations within a typical storage canister by evaluating the properties of a full-diameter cylindrical mockup of an interim storage canister. This mockup has been produced using the same manufacturing procedures as the majority of the fielded spent nuclear fuel interim storage canisters. This document describes the design and procurement of the mockup and the characterization of the stress state associated with various portions of the container. It also describes the cutting of the mockup into sections for further analyses, and a discussion of the potential impact of the results from the stress characterization effort.

In order for SCC to be a viable degradation mode, three criteria must be met – there must be a sufficiently large tensile stress in the material to support crack growth, the material itself must be susceptible to SCC, and the environment must be sufficiently aggressive to support crack initiation and propagation. The work described in this document is aimed at evaluating the first of these criteria for in-service containers by characterizing the material properties of the base metal and weld zones on the canister mockup. Assessment of residual stresses associated with forming and welding was performed using a combination of four techniques. These include deep-hole drilling, the contour method, x-ray diffraction, and ultrasonic testing. The deep-hole drilling technique allows measurement of residual stresses along a one-dimensional hole drilled through the wall of the cylinder; it allows the residual stresses within the container to be assessed while it is intact and hence, captures the effects of the cylindrical constraint on the stresses. The contour method provides a two-dimensional map of stresses along a cross section through a region of interest; however, the mockup must be cut into pieces to measure the face of the cross section, and stresses due to the constraint of the intact cylinder are lost. X-ray diffraction allows assessment of very shallow near-surface stresses associated with shaping and grinding the mockup. It is also used to map stress components that are in-plane with the cross sectional surface, when using the contour method. Ultrasonic testing evaluates the change in sound velocity due to a change in local stress, and is able to evaluate integrated stresses from a depth of 0 to 2.8mm within the stainless steel (as implemented here). The ultrasonic technique is non-destructive, and relatively new as a stress analysis method. It has been included here for comparison to the other techniques discussed above.

After fabrication, the mockup was cut in half. One half was reserved for residual stress measurements. The other half was further subdivided, providing one part for material characterization studies, and the other was provided to EPRI for the assessment of SCC evaluation methods. During the cutting process, strain gauges were used to monitor stress relaxation at locations where weld residual stresses were measured, so that it could be added back in if necessary to obtain the as-manufactured residual stresses. However, measured strains were very small, and can be ignored; cutting the cylinder in half had little effect on residual stresses.

A wide variety of methods are available for residual stress measurement, as summarized in NUREG-2162 (Benson et al., 2014) – both deep-hole drilling (DHD) and the contour method were reviewed as strain-relief based methods that are able to capture the stress distribution through a

thick section. While the contour measurement was found to have issues with steep stress gradients, it provides an overall map of a cross section, whereas, while the DHD technique can be more accurate, it only provides information at a single location. As a result, both techniques were applied to the mockup.

Deep-hole drilling (DHD) measurements were completed within the fusion zone (FZ) and heat affected zone (HAZ) for the circumferential and longitudinal welds. Similar measurements were made in a portion of a circumferential weld that had undergone a repair procedure appropriate for the type of defects seen for submerged arc welds used in structures such as the mockup. A final measurement was performed in the base metal, far from the welds. Results indicate that in regions distant from the welds, residual stresses are dominated by those introduced during the forming of the plate to make a cylinder. The forming process used to shape the stainless steel plates from which the cylinder was constructed extended the outer surface of the shell while shortening the inner surface, and the residual stresses reflect this; except for near-surface regions, the outer half of the shell wall is under tension, while the inner half of the wall is under compression. The stresses associated with the weldments were substantially larger in magnitude than the base metal, with peak values in excess of the uniaxial yield strength for annealed 304L stainless steel. The stress within the weldments is the result of shrinkage during solidification of the molten metal in the weld fusion zone (FZ) upon cooling. These stresses are the result of the constraint placed by the structure of the container (and any additional fixtures used during fabrication) on the weld as it solidifies. *The stresses both within the weld FZ and heat affected zone (HAZ) were found to be strongly tensile through the entire thickness of the container wall*.

Contour measurements were completed across the circumferential weld, the longitudinal weld, and at the intersection of a circumferential weld and longitudinal weld. As with the DHD measurements, the contour measurements indicated that the stress field associated with each of the welds was strongly tensile through the entire wall thickness. The distance over which the stress field remained completely tensile extended approximately 25mm from the weld centerline for longitudinal welds and 40mm from the weld centerline for circumferential. The region of the stress field which was most strongly tensile was narrower for the longitudinal weld, but larger in magnitude, again consistent with the DHD measurements. Looking at the intersection of the two welds, the stress field was similar, save that the tensile region became wider, extending further from the circumferential weld centerline at the location of the intersection.

X-ray diffraction measurements were made on the base metal, on and around the circumferential weld, and at the intersection of the longitudinal and circumferential welds. Unlike the DHD or contour measurement techniques, X-ray diffraction analyzes only the stresses very near (tens of microns) to the sample surface. Since the weld beads for both the longitudinal and circumferential welds, along with the surface near those welds, had been mechanically ground, the stresses were found to be strongly compressive in the near surface region. While compressive stresses would tend to prevent crack initiation, care must be taken in the interpretation of the X-ray diffraction data, as a typical localized corrosion site would be deeper than the stress field that has been measured. As such, the stresses which would be acting on that localized corrosion site, potentially promoting crack initiation, would likely be quite different than the results from x-ray diffraction. While the very near surface stresses may not be important for crack initiation and propagation, they can increase the susceptibility of the material to localized corrosion initiation, and as such should not be dismissed as being irrelevant.

Ultrasonic measurements of the residual stress were made in the same locations as the contour mapping and incremental deep hole drilling measurements. Results obtained, while limited to the shallow sub-surface (representing the integrated stress over a depth of 0 to 2.8 mm from the outer canister surface), were consistent with those reported through the other techniques. As such, while the tooling for ultrasonic measurement, as implemented here, is bulky and doesn't yet lend itself to

inspection of fielded storage containers, it does represent a powerful non-destructive method to evaluate the stress state associated with weldments. Furthermore, implementation of such a technique may be able to reveal the location of weld repairs, where the local stress state may be elevated relative to the steady state portions of a weldment.

Evaluation of the electrochemical properties of the welded regions will be carried out in the future, and will first involve an assessment of the microstructure of the regions at the longitudinal, circumferential, and repair welds via standard metallurgical techniques. The thermal cycling associated with the welding process will, in addition to altering the overall microstructure of the near-weld material, result in the precipitation of chromium carbides and the formation of chromium-depleted regions along the grain boundaries. This effect, known as sensitization, will be particularly pronounced in the weld HAZ (i.e., the region near the weld FZ that has been impacted by heat input from the welding process). The extent to which sensitization has taken place will be documented as a function of position from the edge of the weld FZ. This will be done both for the near-surface regions and through the thickness of the container wall. A volumetric assessment of the degree of sensitization will illustrate the extent of the affected region and illustrate the presence/absence of an active path for crack propagation through the material.

Establishing the storage canister susceptibility to SCC will require assessment of both the crack nucleation and crack propagation processes using samples with relevant crystallographic textures and electrochemical properties, under typical environmental conditions, and at stress conditions as defined by analyses of the full-scale mockup. Several experiments are planned to evaluate crack nucleation and growth, and to determine appropriate methods to produce relevant weld analog materials.

Now that the stress states have been characterized, the mockup will be sectioned into coupons to provide samples for SCC initiation tests. These coupons are critical for the Used Fuel Disposition (UFD) program, but also are of great interest to outside parties such as EPRI and the academic groups working on canister SCC as part of a DOE Nuclear Energy University Program (NEUP). Samples will be disseminated to interested parties on an as-needed basis, with the UFD program getting first priority, followed by the DOE-funded NEUP groups and EPRI.

CONTENTS

FIGURES

TABLES

ACRONYMS

ASME B&PVC	American Society of Mechanical Engineers Boiler and Pressure Vessel Code
ASTM	ASTM International
CHD	Center-Hole Drilling
CISCC	Chloride Induced Stress Corrosion Cracking
DHD	Deep-Hole Drilling
DOE	Department of Energy
EDM	Electric Discharge Machining
EPR	Electrochemical Reactivation
EPRI	Electric Power Research Institute
FCRD	Fuel Cycle Research and Development
FZ	Fusion Zone
HAZ	Heat-Affected Zone
ICHD	Incremental Center-Hole Drilling
iDHD	Incremental Deep-Hole Drilling
ISFSI	Independent Spent Fuel Storage Installation
LANSCE	Los Alamos Neutron Science Center
NDE	Non-Destructive Evaluation
NEUP	Nuclear Energy University Programs
NRC	Nuclear Regulatory Commission
NWTRB	Nuclear Waste Technical Review Board
QA	Quality Assurance
SAW	Submerged Arc Welding
SCC	Stress Corrosion Cracking
SNF	Spent Nuclear Fuel
SS	Stainless Steel
UFD	Used Fuel Disposition
WRS	Weld Residual Stress
XRD	X-Ray Diffraction

FINAL REPORT:

Characterization of Canister Mockup Weld Residual Stresses

1. INTRODUCTION

The potential for stress corrosion cracking (SCC) of welded stainless steel interim storage containers for spent nuclear fuel (SNF) has been identified as a high priority data gap in reviews by the Nuclear Waste Technical Review Board (NWTRB, 2010), the Electric Power Research Institute (EPRI, 2011), the Department of Energy (DOE) Fuel Cycle Research and Development (FCRD) program's Used Fuel Disposition (UFD) campaign (Hanson et al., 2012), and the Nuclear Regulatory Commission (NRC, 2012a, 2012b). Uncertainties exist both in the understanding of the environmental conditions on the surface of the storage canisters and in the textural, microstructural, and electrochemical properties of the storage containers themselves. The canister surface environment is currently being evaluated by Sandia and EPRI (Enos et al., 2013, Bryan and Enos, 2014, EPRI, 2014, Bryan and Enos, 2015); however, little has been done to assess canister material properties and their impact on corrosion. Of specific interest are regions associated with the welds on the canisters, because the welding process modifies the microstructure of the stainless steel as well as its resistance to localized corrosion. In addition, welding introduces high tensile residual stresses that can drive the initiation and growth of SCC cracks. In order to meet the need for additional data on the canister material properties, the UFD campaign has procured a full-diameter cylindrical mockup of a dual certified 304/304L stainless steel (SS) storage canister produced using the same manufacturing procedures as fielded SNF fuel interim storage canisters. The weld and base metal zones on this mockup will be characterized to determine metal properties and susceptibility to SCC. This report documents the mockup specifications and manufacturing processes; the initial cutting of the mockup into three cylindrical pieces for testing and the measured strain changes that occurred during the cutting process; and the weld residual stress characterization results.

Section 2 of this report provides background on the issue of SCC of interim storage canisters and describes the necessary criteria for SCC to occur, in the context of providing rationale for the purchase and analysis of the mockup. Section 3 describes the material, design, quality assurance (QA) specifications, and procurement of the mockup. Section 4 summarizes the planned characterization activities, which are described in detail in the document Technical Work Plan: Characterization of Weld Regions on a Full-Scale Cylindrical Mockup of an Interim Storage Container, FCRD-UFD-2014-000710 (Enos and Bryan, 2014). Section 5 describes the cutting of the mockup, the results of strain measurements performed during the cutting process to monitor relaxation due to cutting, and the results of the stress measurements on the mockup, which have been completed. Finally, Section 6 provides details as to the dissemination of samples from the mockup container to UFD and other research groups evaluating interim storage container performance.

2. BACKGROUND

Following initial cooling in pools, SNF is transferred to dry storage casks for longer-term storage at the reactor sites. The storage cask systems are predominantly welded stainless steel (Hanson et al., 2012) containers enclosed within a ventilated concrete or steel overpack. These cask systems are intended as interim storage until a permanent disposal site is developed, and until recently, were licensed for up to 20 years, and renewals also up to 20 years. In 2011, 10 CFR 72.42(a) was modified to allow for initial license periods of up to 40 years, and also, license extensions of up to 40 years. However, as the United States does not currently have a final disposal pathway for SNF, these containers may be required to perform their waste isolation function for many decades beyond the original design intent. As noted above, several recent analyses (NWTRB, 2010, EPRI, 2011, Hanson et al., 2012, NRC, 2012a) have identified and prioritized potential concerns with respect to the safety performance of long-term interim storage. In each of these studies, the potential for canister failure by chloride-induced SCC (CISCC) was identified as the major concern with respect to canister performance.

2.1 Criteria for Stress Corrosion Cracking

SCC is a localized corrosion phenomenon by which a through-wall crack could potentially form in a canister outer wall over time intervals that are shorter than possible dry storage times. In order for SCC to occur, three criteria must be met (Figure 1): a sufficiently aggressive chemical environment must exist, the metal must be susceptible to SCC, and sufficient tensile stress must be present to support SCC. In general, these criteria are expected to be met, at least at some Independent Spent Fuel Storage Installation (ISFSI) sites, during the period of interim storage.

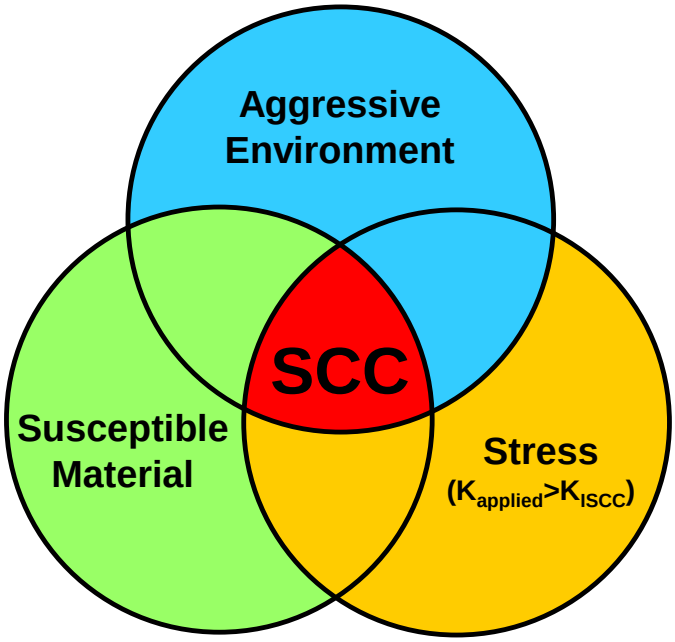

Figure 1: Criteria for SCC initiation and propagation.

Aggressive chemical environment: Field sampling of surface deposits on in-service SNF storage canisters at three near-marine ISFSI sites has been carried out in recent years, and analyses have shown that chloride-rich salts can be present on the canister surfaces (Enos et al., 2013, Bryan and Enos, 2014, EPRI,

2014, Bryan and Enos, 2015). Once portions of the canister surfaces cool sufficiently for these salts to deliquesce, a potentially corrosive, chloride-rich aqueous brine layer could form locally on the canister surface.

Susceptible material: The majority of SNF dry storage casks currently in use are made from austenitic stainless steels, including 304, 304L, and 316. Should sufficient tensile stress be present, there is ample evidence that these stainless steels are susceptible to CISCC in sufficiently aggressive chloride-bearing environments. SCC of 304 SS, the most widely used alloy for containers that are currently in service, has been observed in laboratory tests utilizing deliquesced sea-salts (e.g., (Nakayama, 2006, Prosek et al., 2009, Tani et al., 2009, Mintz et al., 2012, Prosek et al., 2014), and has also been observed in near-marine ambient temperature field tests and industrial sites (Kain, 1990, Hayashibara et al., 2008, Kosaki, 2008, Cook et al., 2011, Nakayama and Sakakibara, 2013, Cook et al., 2014). However, overall susceptibility is a function of several factors, including the metallurgical condition of the steel (e.g., degree of sensitization near weldments, etc.), the degree of cold work, and the surface finish (Parrott and Pitts, 2011); to date, none of these factors have been assessed for materials representative of fielded interim storage canisters. While these factors are known to affect susceptibility to SCC, they are all specific to the material and to the manufacturing processes used to fabricate the canister, hindering drawing direct conclusions for specific regions on the mockup from the data found in the literature. In order to evaluate them, it is necessary to obtain relevant metal samples, from a canister or mockup made using the same techniques as real, in-service canisters.

Tensile stress: In order for an SCC crack to initiate, the tensile stresses in the metal must be of a sufficiently large magnitude that the threshold stress intensity value at a potential nucleation site is exceeded. In order for an initiated crack to propagate and penetrate through the container, the applied stress intensity at the crack front must be maintained above that threshold. In other words, a sufficiently large tensile stress state must exist through the entire wall thickness. Tensile stresses may be applied externally—for instance, by loading or by pressurization—but for SNF interim fuel canisters, external loads are a small fraction of the yield stress of the metal, and thus unlikely to provide sufficient driving force for crack initiation/propagation. High residual tensile stresses may be present in the metal, however, due to cold working or welding. Weld residual stresses (WRS) are generally the most important component, and are a function of many factors, including weld geometry, sample thickness, welding speed, number of passes, inter-pass temperatures, and base metal properties relative to the weld. Because of this, WRS are specific to the geometry and welding processes used, and can only be measured from an actual storage canister or a mockup made using the same procedures as the real canisters. However, WRS measurements on samples with relevant geometries and typical welds have never been done. The NRC modeled WRS for typical canister welds using finite element methods (NRC, 2013), and predicted that within the heat affected zone (HAZ) of both longitudinal and circumferential welds, sufficient tensile stresses would be present to support SCC. Moreover, they predicted that the tensile stresses would be present through the thickness of the cylinder wall, permitting full penetration over time.

2.2 Need for a Full-Sized Mockup

The DOE has recognized that evaluation of the material susceptibility and weld residual stresses in interim storage canisters is critical to understanding the implications of the potentially corrosive environment that may develop on the surface of the canisters. These material properties control the likelihood of SCC initiation, and ultimately, the rate at which any nucleated crack will grow should SCC develop, along with the potential for crack stifling prior to penetration. For this reason, the DOE has purchased the full-diameter cylindrical mockup evaluated in this document, made using materials and manufacturing procedures identical to those used to fabricate one particular in-service storage canister design. The canister mockup is being characterized using a suite of different techniques, with the goal of determining the following:

1. The near-surface and through-thickness residual stress states associated with the welds used to construct the container
2. Stress states near typical weld repair zones, two of which were produced on the mockup.
3. The near-surface and through-thickness residual stress states associated with the as-formed walls of the container (i.e., far from the welds)
4. The degree of sensitization associated with the various weldments used to form the container
5. Textural and metallurgical characteristics of the welds and HAZ, and changes in the near-surface metal of the canister shell due to cold-working, and their potential impact on the corrosion properties of the metal.

Characterization of the residual stresses, the first three bullets, has been completed, and is documented in this report. The additional characterization work will be documented in future reports.

3. DESIGN AND PROCUREMENT

The material properties that will be measured are strongly controlled by the materials and manufacturing processes used to make the interim storage canister. Therefore, the mockup had to be made using the same materials and fabrication methods as a real canister. Nearly all storage canister designs use 304 SS (for older containers) and welding is multi-pass, predominantly utilizing the submerged arc welding process with a double-V edge preparation. To ensure consistency with a real canister design, price quotations were requested from the three major cask vendors. Areva-TN (formerly TransNuclear) makes horizontal canister storage systems, and their NUHOMS systems account for about 38% of all storage systems presently deployed in the US. HOLTEC International and NAC International manufacture vertical canister storage systems, and account for about 35% and 23% of all current canister systems, respectively. However, HOLTEC and NAC did not submit a bid. Areva-TN did not respond directly, but instead recommended that Ranor Inc. be contacted. Ranor is an industrial manufacturing/fabrication facility that in the past has been contracted to build stainless steel storage canisters for TransNuclear. With the permission of Areva-TN, Ranor was willing to build the mockup using identical materials and procedures as were used to build the original TransNuclear horizontal storage canisters. Ranor was ultimately contracted to build the mockup. Use of the same manufacturer was critical as, while the overall design is owned by Areva-TN, the production methodologies used are proprietary to Ranor. That is, Areva-TN specified the overall design (i.e., material, overall dimensions, etc.) but Ranor developed the methodology to actually build each storage container.

Three plates of dual-certified 304/304L SS were used to construct the container. The thickness of each plate was verified via ultrasonic inspection prior to being welded. The weld filler metal was 308L SS, as typically used when welding 304 SS. The compositions of the 304/304L SS plates and the 308L SS filler material are in Table 1 below. In addition to the composition of the materials of construction, the parameters for each weld pass were documented in the data package provided with the mockup. These include the current, voltage, travel speed, heat input, and interpass temperature. X-ray films of all welds and weld repairs were also included in the data package.

Table 1: Composition of 304L Plate and 308L Filler Metal Used to Construct Mockup

	C	Co	Cr	Cu	Mn	Mo	N	Ni	P	S	Si
Plate Material (304/304L)	0.0223	0.1865	18.1000	0.4225	1.7125	0.3180	0.0787	8.0270	0.0305	0.0023	0.2550
Weld Filler (308L) (lot 1)	0.014	--	19.66	0.16	1.70	0.11	0.058	9.56	0.025	0.010	0.39
Weld Filler (308L) (lot 2)	0.012	--	19.71	0.192	1.730	0.071	0.053	9.750	0.024	0.012	0.368

The mockup whose evaluation is described in this document is based upon the TransNuclear NUHOMS 24P design (Pacific Nuclear Fuel Services, 1991). This container design is employed at the Calvert Cliffs nuclear power station, which was the first site surveyed by EPRI for the dust composition on the surface of the containers (Gellrich, 2013). The mockup, pictured schematically in Figure 2 below, consists of three cylindrical shells, each 48 inches long and 67.2 inches in diameter, and having a wall thickness of 5/8 inch. Each shell was formed by cold forming a plate into a cylinder, then making a single longitudinal weld to form the cylinder. The three cylinders were then welded together to form a single large cylinder 12 feet in length with two circumferential welds. All of the welds were formed via the submerged-arc welding (SAW) process and were multi-pass. The edge preparation used for each weld was a 30 degree bevel, with a quarter inch land, as illustrated in Figure 3 below. Each inner-diameter weld consisted of three passes, and with one exception, each outer-diameter weld was made with four passes (the exception had 5). The inner diameter was welded first, followed by the outer diameter. Once

the inner diameter weld was made, the edge preparation for the outer diameter weld was made by arc-gouging along the parting line between the two plates being welded together. The depth of the gouge was adjusted such that the parting line was no longer visible, ensuring there would be no voids/gaps. Detailed weld parameters are presented in Table 2 and Table 3 for the longitudinal and circumferential welds, respectively. As seen in the table, welds were made at a rate of 15 to 16 inches per minute at a voltage of 30V and current of 400A. Typical heat input was 45 kJ/in. A representative cross sectional image of a circumferential weld is presented in Figure 4 below. During analysis of the residual stress state associated with the weld, it was noted that the outer diameter weld appeared to be misaligned relative to the inner diameter weld. As can be seen in Figure 4, the final weld passes were somewhat asymmetric, and as such the weld toe on the outer diameter of the container did not align with the weld toe of the inner diameter. However, the cross section of the weld revealed a well-formed weld joint, consistent with the volumetric inspection performed by Ranor. As such, later in the text when stress distributions are presented, a weld centerline will not be indicated as it was not possible to ascertain the centerline based upon the appearance of the inner or outer diameter welds. Upon completion of the welding, the surface of each weld was smoothed, following the procedures developed by Ranor. This grinding, along with handling marks, etc. (illustrated in Figure 5) will likely have a significant impact on the near-surface stresses in the weld and nearby regions.

Table 2: Weld Parameters for Longitudinal Welds

	Interpass temperature (°F)	Amperage	Voltage	Travel Speed (IPM)	Heat Input (J/in)
Weld Joint 1 (WJ-1)					
ID - Pass 1	74	400	30	15.4	46753
ID - Pass 2	199	400	30	15.42	46755
ID - Pass 3	214	400	30	15.4	46753
OD - Pass 1	69	400	30	15.16	47493
OD - Pass 2	104	400	30	15.16	47493
OD - Pass 3	110	400	30	15.16	47493
OD - Pass 4	177	400	30	15.16	47493
Weld Joint 2 (WJ-2)					
ID - Pass 1	76	400	30	15.4	46753
ID - Pass 2	161	400	30	15.4	46753
ID - Pass 3	181	400	30	15.42	46755
OD - Pass 1	75	400	30	15.16	47493
OD - Pass 2	148	400	30	15.16	47493
OD - Pass 3	187	400	30	15.16	47493
OD - Pass 4	155	400	30	15.16	47493
Weld Joint 3 (WJ-3)					
ID - Pass 1	76	400	30	15.48	46512
ID - Pass 2	161	400	30	15.4	46753
ID - Pass 3	181	400	30	15.4	46753
OD - Pass 1	75	400	30	15.16	47493
OD - Pass 2	123	400	30	15.16	47493
OD - Pass 3	122	400	30	15.16	47493
OD - Pass 4	210	400	30	15.16	47493

Table 3: Weld Parameters for Circumferential Welds

	Interpass temperature (°F)	Amperage	Voltage	Travel Speed (IPM)	Heat Input (J/in)
Weld Joint 4 (WJ-4)					
ID - Pass 1	70	400	30	16.4	43902
ID - Pass 2	199	400	30	16.4	43902
ID - Pass 3	214	400	30	16.4	43902
OD - Pass 1	74	400	30	15.8	45454
OD - Pass 2	85	400	30	15.8	45454
OD - Pass 3	110	400	30	15.8	45454
OD - Pass 4	88	400	30	15.8	45454
OD - Pass 5	97	400	30	15.8	45454
Weld Joint 5 (WJ-5)					
ID - Pass 1	77	400	30	16.4	43902
ID - Pass 2	126	400	30	16.4	43902
ID - Pass 3	135	400	30	16.4	43902
OD - Pass 1	68	400	30	15.1	47682
OD - Pass 2	102	400	30	15.1	47682
OD - Pass 3	176	400	30	15.1	47682
OD - Pass 4	160	400	30	15.73	45772

In addition to welds formed under nominal conditions, discussions with TransNuclear and Holtec have indicated that during construction of actual storage containers, repairs are commonly necessary at regions along the welds where the nondestructive testing indicated that the weld did not conform to the criteria in ASME B&PVC Section III, Division 1, Subsection NB. Repair regions have been identified by numerous researchers as having dramatically elevated residual stresses when compared to unrepaired portions of a weld (Dong et al., 2002, Bouchard et al., 2005, Dong et al., 2005, Elcoate et al., 2005, George and Smith, 2005, Hossain et al., 2006, Hossain et al., 2011). During fabrication of the mockup, all of the welds were subjected to a full radiographic inspection, and no indications requiring repair were found. However, because of the potentially important effect of weld repairs on weld residual stresses and material properties, one region on each circumferential weld was subjected to a repair procedure representative of what would typically be done for a SAW weld on the outer diameter. In these locations, an artificial defect corresponding to a 1/8" diameter hole was drilled partially into the outer diameter, simulating a small defect such as porosity or an entrained slag particle (illustrated schematically in Figure 6). The "defect" was then removed by machining out a larger region via a ¼" drill, after which the edges of the drilled out region were ground to a bevel, such that it could be re-welded. The repair was welded using the gas tungsten arc welding technique. Characterization of these sites will allow determination of weld residual stresses and degrees of sensitization typical of weld repair regions.

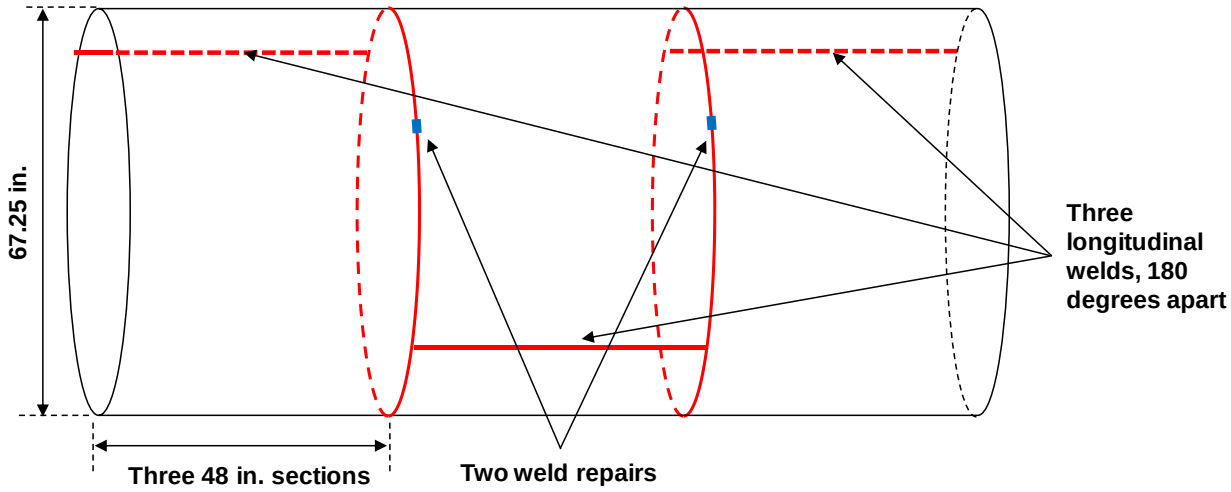

Figure 2: Schematic representation of the full scale mock storage container manufactured at Ranor

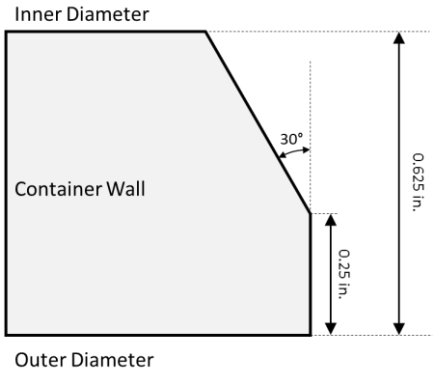

Figure 3: Edge preparation prior to welding used for both circumferential and longitudinal welds.

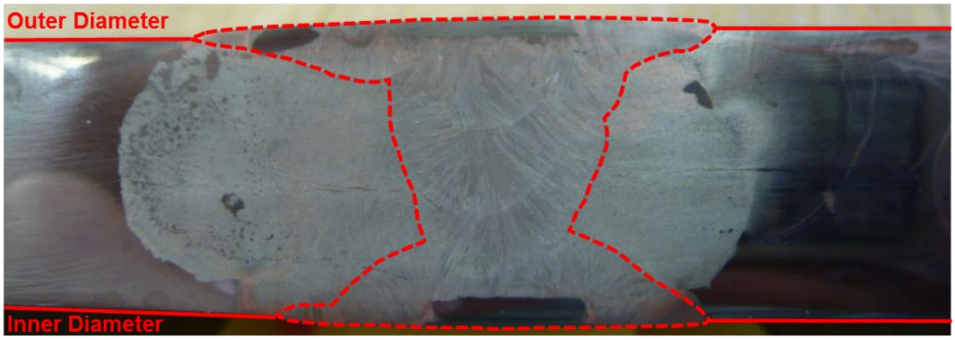

Figure 4: Cross section of a longitudinal weld. Note that the outer diameter FZ passes well into the initial weld made on the inner diameter. Also note that the final weld passes were sometimes offset from the centerline of the weldment, yielding an asymmetric appearance.

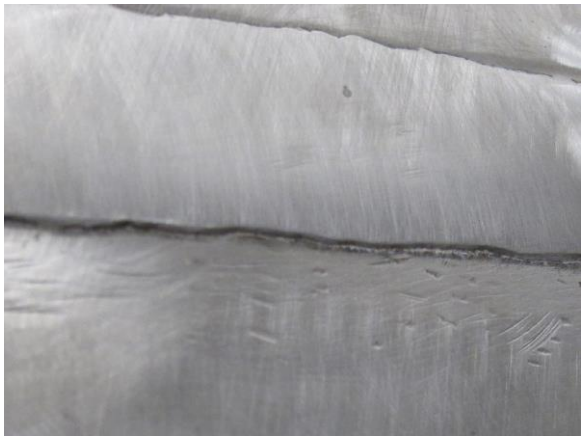

Figure 5: Grinding and machining marks associated with a circumferential weld. This treatment will significantly impact the near surface stresses associated with the processed regions.

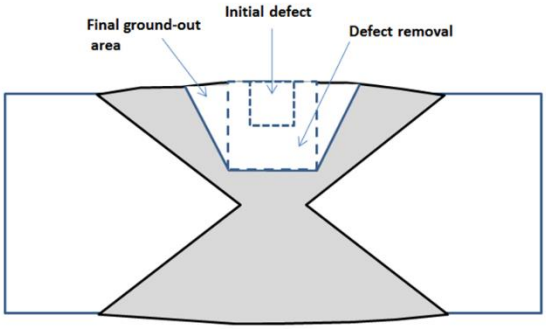

Figure 6: Schematic representation of simulated defect placed in each of the circumferential welds. Once the "defect" was removed, the region was re-welded using the gas tungsten arc welding technique

4. RESIDUAL STRESS CHARACTERIZATION METHODS USED ON THE MOCKUP CONTAINER

In addition to a susceptible material and a sufficiently aggressive environment, the nucleation and growth of a stress corrosion crack requires the presence of a sufficiently large stress. In the case of interim storage containers, the stress existing within the structure will predominantly be residual stresses resulting from the forming of the metal plates into a cylinder and the subsequent welding and associated solidification shrinkage of the FZ upon cooling. The latter are likely to be the largest in magnitude, and are the result of the constraint placed by the structure of the container (and any additional fixtures used during fabrication) on the weld as it solidifies. A wide variety of methods are available for residual stress measurement, as summarized in NUREG-2162 (Benson et al., 2014). Techniques are typically based on measurement of elastic strains in the crystal structure using diffraction of either x-rays or neutrons, or on strain measurements made by mechanically altering the material being investigated (allowing stress relaxation to occur). The techniques vary in terms of their sensitivity and depth of penetration into the substrate metal. The most appropriate technique for assessing the mockup storage container is one capable of measuring the stresses through the thickness of the container wall. Furthermore, the technique must allow for evaluation of large sections, as it is desired that the stress state be measured prior to and following the sectioning of the container into smaller samples for use in localized corrosion or SCC experiments.

Four techniques were used in this study. These include deep-hole drilling (DHD), the contour method, x-ray diffraction (XRD), and ultrasonic stress measurement. *In-situ* neutron diffraction was initially explored via collaboration with Los Alamos National Laboratory (LANL), and was called for in the initial test plan (Enos and Bryan, 2014). The analyses were to be performed at the Los Alamos Neutron Science Center (LANSCE) at Los Alamos National Laboratory. However, because of funding reductions at LANSCE, it is no longer a user facility and became unavailable for use in this program. As no other neutron beam facility in the country is capable of handling a steel ring 6 feet in diameter, plans to analyze mockup weld residual stresses by using neutron diffraction were shelved.

4.1 Deep-Hole Drilling

A variety of hole-drilling based techniques are available for the evaluation of the stress state in a metal sample. Typically, these techniques involve the attachment of strain gauges to the surface of the material being measured, which are monitored while a hole is precisely drilled in the material. As the hole is drilled in depth increments, the local constraint within the structure is relaxed, allowing stress relaxation to occur, resulting in surface deformation which is captured by the strain gauges. This method is known as incremental center-hole drilling (ICHD). A similar drilling technique involves the use of a surface strain gauge around which a core is cut into the material, allowing the center pillar to relax. These techniques, while they can be accurate, are only sensitive to the near-surface stresses in the material.

The DHD methodology differs from other hole-drilling techniques in that it does not rely on the use of surface strain gauges. The technique is illustrated schematically in Figure 7. Initially, a bushing made of a material similar to the material being evaluated is attached to either side of the sample. Next, a small-diameter hole is precisely drilled via a gun drill through the material, starting at one bushing, passing through the material of interest, and then exiting through the back bushing. An air gauge is then used to precisely characterize the diameter of the hole along its length. Next, electric discharge machining (EDM) is used to cut an over-core around the gun-drilled hole. As the core is cut, the constraint placed on the metal immediately adjacent to the central hole is relaxed, resulting in local lateral displacement of the material. The inner diameter of the hole is then re-characterized and the resulting change in diameter, due to the loss of constraint around the hole, is recorded. From these strains, the original residual stress state within the material as a function of depth can be calculated. The DHD technique is not sensitive to near-surface stresses, and hence is commonly combined with ICHD to obtain a full through-thickness weld residual stress profile, if near-surface stresses are of interest.

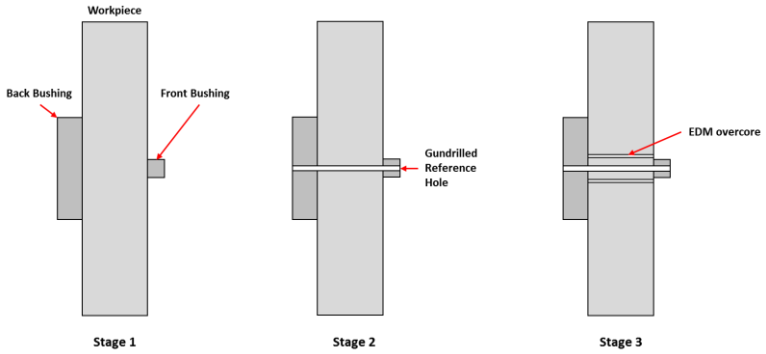

Figure 7: Schematic representation of the physical steps involved in a deep hole drilling measurement. First, bushings are attached on either side of the workpiece, then a precisely define hole is drilled through the workpiece and its diameter characterized along its length. Finally, an EDM over-core is performed, releasing the aforementioned hole from the structure. The resulting dimensional changes of the hole are then used to calculate the pre-existing residual stress state.

The calculations used for standard DHD are based upon the assumption that the stress relaxation leading to the measured displacements is entirely elastic in nature. When large stresses are present, this is not true, and plastic deformation of the material can result, hindering the ability of the technique to resolve stress. For a heavily constrained weld, such as the circumferential weld on the interim storage containers, it is anticipated that the residual stress levels will be very high – approaching the yield strength of the material – and as such, the traditional analysis will not work. To compensate for this, the DHD technique must be modified (Mahmoudi et al., 2009, 2011). In the modified technique, the EDM core is cut in steps. After each step, the inner diameter of the hole is characterized via the air probe. By measuring the deformation of the inner diameter of the hole at the depth of the core cut, the effect of plasticity can be addressed. The resulting residual stress distribution, while being lower in vertical resolution than the traditional measurement, is able to resolve large residual stresses. This modified technique is known as incremental deep-hole drilling (iDHD).

The DHD technique is semi-destructive in nature. The drilling of the hole and the EDM overbore is locally destructive, but the site is small (1.5mm diameter hole, 6mm diameter overbore), and the remainder of the structure being evaluated is undisturbed. Perhaps more importantly, the deep hole drilling technique can be employed without cutting the mockup into smaller pieces.

The contour method, described below, analyzes a cross-sectional surface of the metal, which requires cutting a section of the weld from the mockup. While the use of surface strain gauges can help measure the stress relaxation associated with cutting a section from the mockup, the cutting process introduces an additional level of uncertainty to the residual stress measurement.

As the DHD technique is inaccurate near the outer metal surface, CHD or ICHD (described previously) was used to measure the stresses in the first 0.5mm of material. In this technique, a strain rosette similar to that pictured in Figure 8 is placed on the surface to be analyzed, and then a hole is precisely drilled through the center of the pattern. The positioning of the drilling tool is illustrated in Figure 9a, and the resulting hole, surrounded by the strain gauge rosette, is shown in Figure 9b. As the hole is drilled, the stress relaxes in the region near the hole, the resulting strains from which are monitored by the strain gauges described above. These strains are then converted to the effective stresses near the surface.

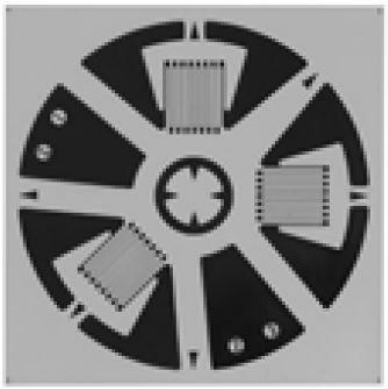

Figure 8: Strain gauge rosette used to perform ICHD measurements. As the hole is drilled at the circular indication in the center of the pattern strains are measured in three directions, with the strain gauges positioned at 0, 90 and 225 degrees.

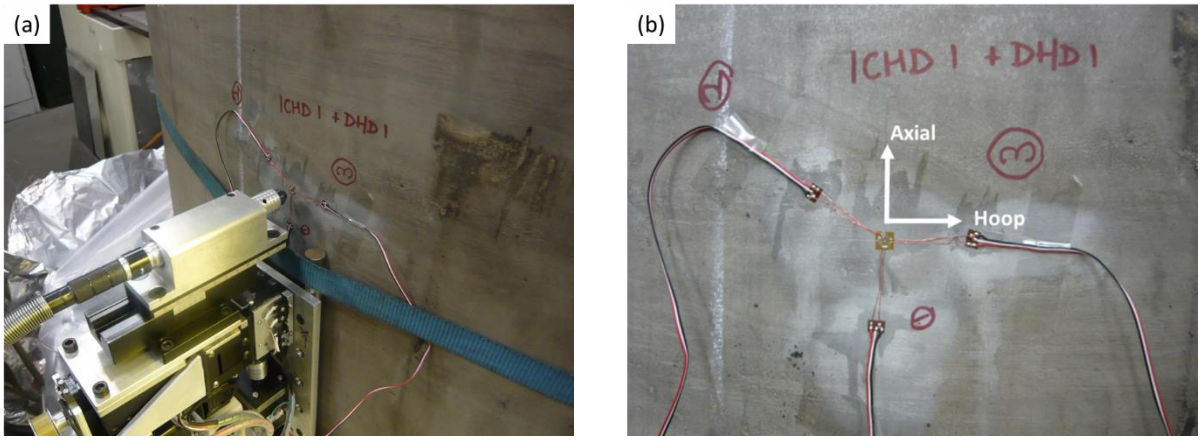

Figure 9: Mechanism used to perform ICHD measurements in the base metal (far from the longitudinal and circumferential welds). Drilling equipment is shown in (a) and the orientation of the strain gauge relative to the axial and hoop directions is illustrated in (b).

4.2 Contour Method

As with hole drilling techniques, the contour method involves the removal of constraint from the system, and the measurement of the resulting relaxation displacements. The contour method is similar to the deep hole drilling method in that displacements due to elastic stress relaxation are converted to a pre-existing residual stress. It is critical that any stress relaxation that takes place as the sample is cut from the structure (e.g., removing a section of a weld from the overall mockup) due to the loss of constraint provided by the surrounding structure, is accounted for. The process is illustrated in Figure 10 for a contour measurement made for a longitudinal weld. First, surface-mount strain gauges were placed on the surface in the region where the contour measurement will be made. The mockup was then cut, and the segment of the weld to be evaluated was removed from the overall structure. A sacrificial bushing was adhered onto both sides of the region being contoured, to keep the section being cut uniform in thickness and to reduce wire-EDM surface cutting artifacts. Next, the sample is rigidly held within a

wire-EDM (electrical-discharge machining) machine, and cut into two sections in a single pass with a 250μm diameter brass wire on "skim cut" settings. The cut creates two stress-free surfaces and hence relaxes the out-of-plane residual stresses in the region of interest. A coordinate measuring machine was then used to precisely measure the deviations of the cut surface resulting from the stress relaxation associated with making the cut. Mathematically, the deviations (i.e., strains) were then converted into the residual stress state that existed prior to being cut. In essence, the amount of stress required to force the surface flat is calculated.

The calculated stress field represents one stress direction – perpendicular to the cut surface. In order to get stresses within the plane of the cut surface, XRD measurements are made, mapping the other two stress states over the exposed surface. The contour surface was first electrolytically etched to remove the recast region from the EDM cut, then XRD measurements were performed.

The contour method is destructive in nature and requires that the region being measured be extracted from the mockup container. The use of external strain gauges when extracting the sample enables the stress relaxation not captured by the contour measurement itself to be added back in, such that the initial stress state can be accurately estimated. By combining this method with iDHD prior to cutting, changes in stress due to cutting can be even more accurately estimated and corrected for, resulting in a high-resolution map of the stress distribution across the entire cut surface.

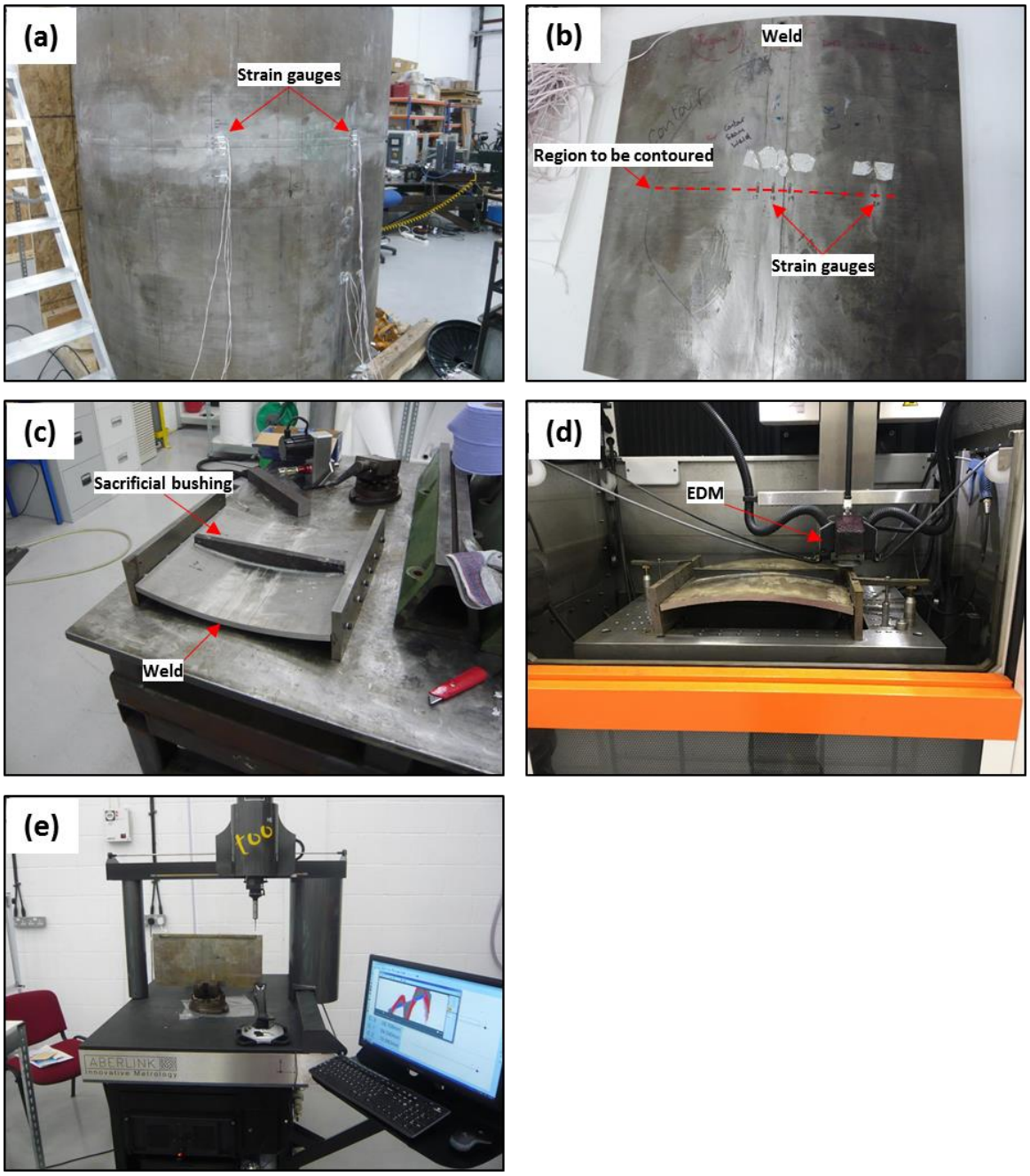

Figure 10: Illustration of the steps associated with making a contour measurement of a weld on the mockup container. First, the surface is instrumented with strain gauges (a), after which the region to be contoured is cut from the mockup (b). Next, sacrificial bushings are attached to the front and back of the region to be contoured (c) and then the sample is rigidly secured in place, and an EDM is used to cut the contour region (d). Finally, the cut surface is measured with a coordinate measuring machine (e).

4.3 X-Ray Diffraction

Diffraction-based measurements allow the stress state to be evaluated with little or no cutting of the material being evaluated. Due to the low penetration depth of x-rays into the metal being evaluated, only

the very near surface stresses can be measured (i.e., tens of microns into the sample). An x-ray source is directed towards the surface being analyzed. The x-rays are then diffracted by the atomic structure of the stainless steel. Using Bragg's law, the diffracted x-rays are used to measure the lattice spacing of the stressed sample. Through the use of differential analysis techniques, the need to obtain data from an unstressed control (as required for neutron diffraction) is not needed for x-ray diffraction. Based upon the distortion of the stressed sample (in terms of the change in lattice spacing relative to unstressed material), the strain field within the structure can be determined. These strains are then converted to normal stresses through the use of Hooke's law in two dimensions.

4.4 Ultrasonic Measurements

The UT residual stress measurement technique exploits the acousto-elastic property of materials, in which the speed of sound through a material changes with stress. The speed of a longitudinal ultrasound wave through a material has been determined to be sensitive to stress changes in the direction of propagation of the wave. In essence, the speed of the longitudinal wave decreases in regions where a tensile stress exists, and increases in regions where the stress is compressive in nature. As such, effective quantitative application of this technique requires that an unstressed segment of material of similar microstructure and composition as the stressed region being assessed be analyzed, similar to techniques such as neutron diffraction.

The sound velocity within the stainless steel wall was evaluated in a volume with a depth of approximately 2.8mm, approximately 16mm long, and 6mm wide. The sound velocity is then compared to the velocity in an unstressed sample of the material, and the local stress is then proportional to the change in velocity due to the residual stress present within the material. Only the residual stresses in the hoop direction were measured via the UT system. Performing the test was accomplished by first placing an ultrasonic couplant over the measurement location (to allow coupling of the sound waves from the transducers located within an acrylic test fixture, and the stainless steel). The transit time between ultrasonic transducers positioned at each side of the gauge length was measured via an oscilloscope, the resulting velocities were then calculated and used to determine the stress state at each measurement location. The measurement fixture was moved across each measurement location, allowing the variation in residual stress to be measured as a function of position.

4.5 Stress Measurement Locations on the Mockup

In order to completely characterize the residual stresses associated with the welds in the mockup, a combination of the techniques described above has been employed. Combining the measurements will mitigate the errors/uncertainties associated with any one method. The container was cut at Ranor in the center of the middle segment (i.e., at the midpoint between the two circumferential welds) as shown in Figure 11. The mockup was placed on a rotary table, and a 1 inch roughing end mill was used to cut around the circumference. Each cut was made in four segments, with an 0.25" ligament left intact between each segment to assist with positioning of the container. Once the milling was complete, the four ligaments were cut, separating the two sections. One section was sent to the facility performing all of the residual stress measurements, VEQTER Ltd. of Bristol, United Kingdom. During the cutting process, surface-mounted strain gauges were used to measure relaxation that might occur due to loss of constraint, so that it can be added back into the measured residual stresses later, if necessary. The other half of the mockup was further subdivided to be used for other characterization and testing activities, as described later in this report (Section 7).

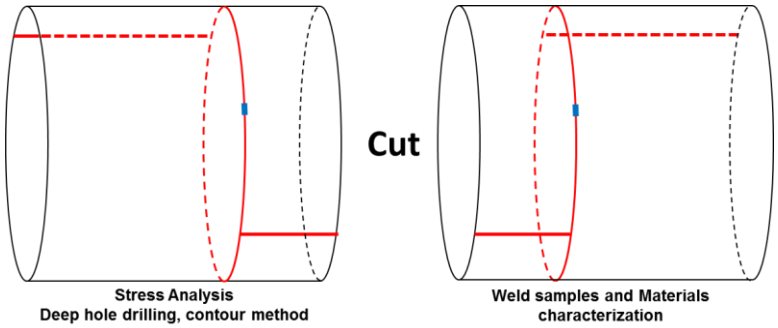

Figure 11: Plan for sectioning the container into two segments, one for weld samples and materials characterization and the other for residual stress measurements using DHD and contour method measurements.

Measurements were made in five different regions, as illustrated schematically in Figure 12. These regions include representative circumferential and longitudinal weld sections, and a repair region. Finally, the stress state of the base metal was measured. The following measurements were done.

Welds:

a. iDHD measurement in center of FZ of both a longitudinal and circumferential weld
b. iDHD measurement in the HAZ (immediately adjacent to FZ) of both a longitudinal and circumferential weld
c. Contour measurement perpendicular to weld centerline of both a longitudinal and circumferential weld
d. Contour measurement through the intersection of a circumferential and longitudinal weld (parallel to the centerline of the longitudinal weld)
e. XRD scan across the circumferential weld
f. XRD scan across the intersection of a longitudinal and circumferential weld
g. Ultrasonic scan across a longitudinal and a circumferential weld
h. Ultrasonic scan across the intersection of a longitudinal and circumferential weld

Weld repair:

a. iDHD measurement in center of weld FZ (center of repair)
b. iDHD measurement in the HAZ on either side of the repair.

Base metal:

a. DHD measurement
b. X-ray diffraction scan in several locations to observe surface stresses

In addition to the measurements described above, a single deep-hole (just the gundrilled portion of a DHD measurement) was made into a longitudinal and circumferential weld. These holes were evaluated before and after segmenting the container. These measurements will provide an assessment of the degree of stress relaxation associated with the loss of constraint of the container as it is sectioned, and will be critical in assessing the validity of measurements performed on unconstrained plates.

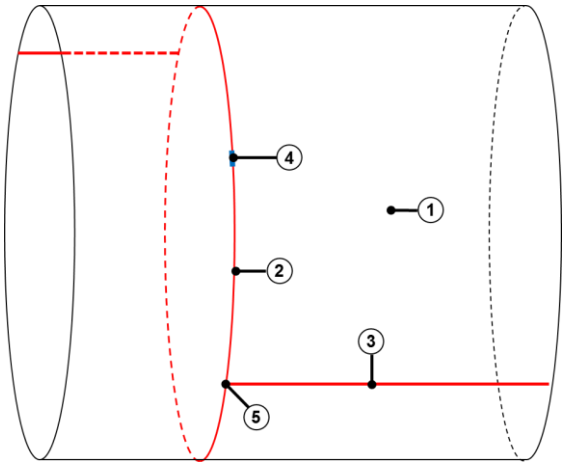

Figure 12: Regions for residual stress measurements. (1) Base metal, (2) Circumferential weld, (3) Longitudinal weld, (4) Weld repair region, and (5) Weld intersection.

5. RESULTS OF THE RESIDUAL STRESS CHARACTERIZATION STUDY

5.1 Sectioning of the Mockup

As described in the previous sections, the mockup cylinder will be used in several different ways. One main goal is to measure weld residual stresses, and this must be done on a large cylindrical section of the mockup, in order to capture the effects of the cylindrical constraint on the stresses. Other parts of the mockup will be used for material characterization studies, and for testing techniques for non-destructive evaluation (NDE) of canister surfaces for SCC cracks. The mockup has been subdivided into three sections, as indicated in Figure 13. The largest of the three sections has been used to assess the residual stress state of the weldments and base metal using techniques described in Section 4 and detailed below for this specific application. The second section will be cut into pieces to provide samples of both the longitudinal and circumferential welds to the UFD program for the assessment of SCC susceptibility. The first section will also be cut into samples upon completion of residual stress analyses. The final section was taken from the base of the container and was provided to EPRI as a mockup for testing NDE techniques. The location of each section on the actual mockup is shown in Figure 14a.

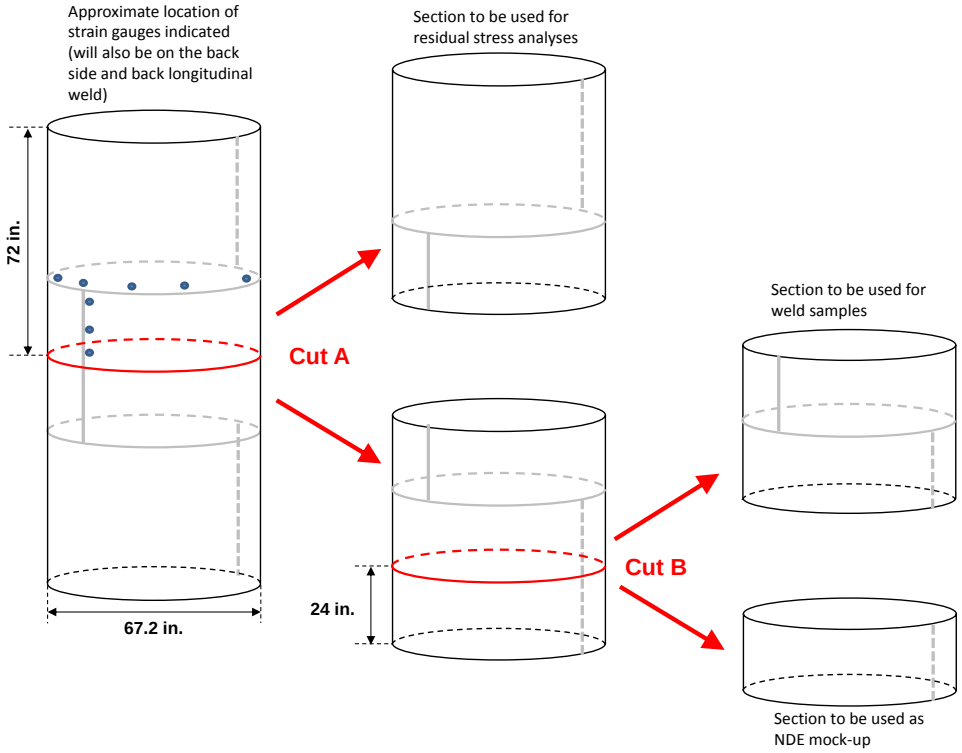

Figure 13: Cut plan used to subdivide the container into sections for residual stress analysis and test coupons.

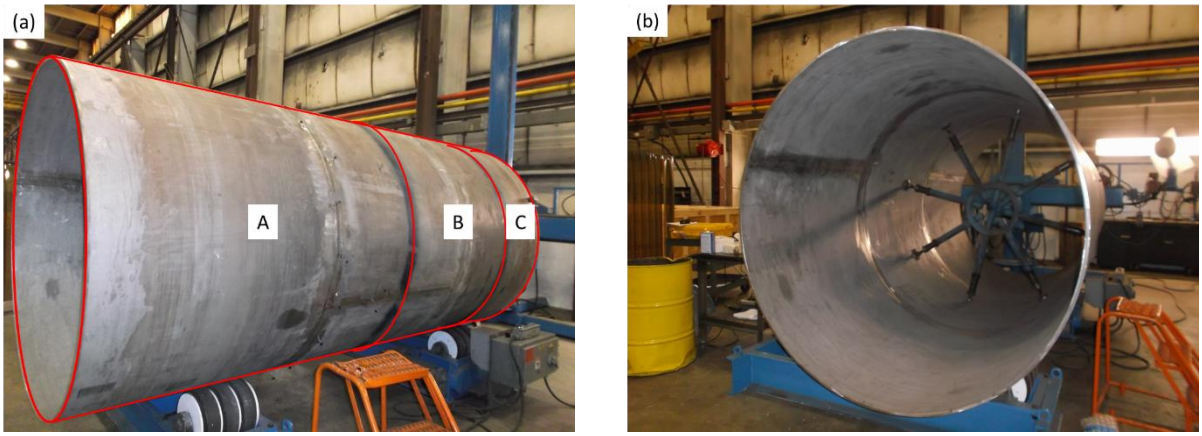

Figure 14: Mockup container prior to being sectioned. (a) Location of three sections into which the container was cut – one for residual stress analysis (A) and two for specimens (B and C). A temporary spider (b) was placed just below the cut made between sections A and B in order to minimize distortion as the cut was made.

Cutting of each section was performed using a 1" roughing end mill. Each cut was made as a series of four smaller cuts, leaving an approximately 0.25" ligament between each cut. These ligaments served to stabilize the container while cutting. In addition, to minimize distortion within the container, the container was reinforced internally using a spider as shown in Figure 14b. The spider was positioned immediately below the cut between the upper section (to be used for residual stress analysis) and the lower section (to be used for specimens). The spider was temporary and removed upon completion of the cut, leaving no visible deformation upon removal. In addition to the spider, four temporary blocks were welded to the end of the container to allow it to be secured to the rotary table used during the cutting operation. These blocks were 1" x 2" x 3" in size and were removed upon completion of the cut. All four are located on the lower section designated "C" in Figure 14,and were far from any locations used for surface strain measurement, as illustrated in Figure 15.

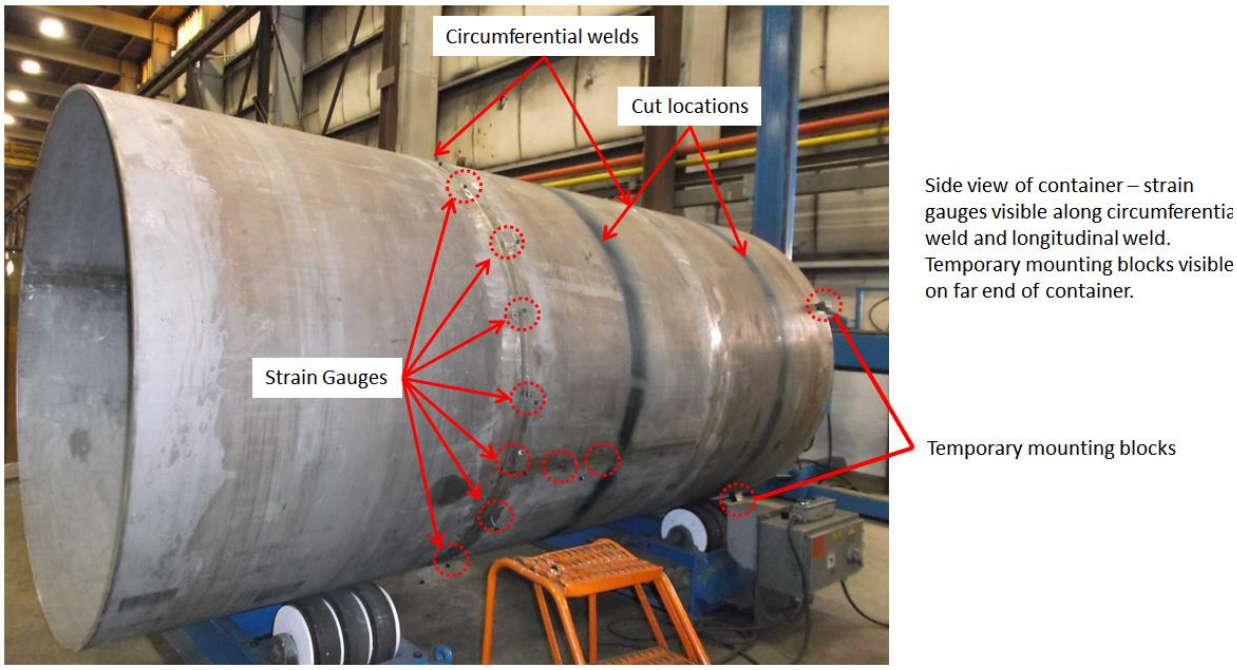

Figure 15: Location of surface strain gauges positioned along the longitudinal and circumferential welds. Also shown is the position of the temporary mounting blocks welded to the base of the container to facilitate positioning while the cuts were being made.

There are two primary sources of residual stress within the container, the origin of which is best illustrated by a discussion of how the cylinder was formed. The raw material used to form each of the three segments of the cylinder was received in the form of annealed plate. These plates were then deformed into a cylinder – a process which is accomplished by gradually bending the plate, introducing significant plastic deformation of the material, and a complex stress state through the thickness of the wall. Once formed into cylinders, each plate was then welded. When the weld is made, the liquid metal in the weld pool solidifies, and in the process, contracts. Since this contracting material is effectively held in place (i.e., constrained) by the overall structure of the cylinder, the degree to which the solidifying metal can contract is limited, and as a result the solidified weld has a considerable tensile residual stress. Similarly, the material away from the weld root is also impacted by the attempted contraction of the weld, and as a result it is under a compressive residual stress. It is the combination of these two stresses (formation and welding) that form the driving force for any potential SCC. When the container is subdivided by cutting, the constraint on which each portion of the container by the overall structure is changed, allowing for macroscopic deformation as the stresses relax. In order for the stresses within the as-manufactured container to be measured accurately, any such relaxation due to the cutting operation must be measured and accounted for.

To measure any relaxation that occurred during cutting, surface-mount strain gauges were positioned along the longitudinal and circumferential welds at 10 inch intervals. While relaxation might be greater closer to the cut, the weld regions are the critical areas, as they are where WRS will be later be measured. A total of 28 strain gauges were utilized. In Figure 15, the position of some of these gauges is illustrated. The gauges themselves consisted of two designs procured from Vishay Precision Group, and are illustrated in Figure 16. Each strain gauge is a tee rosette consisting of two separate sensors, one of which was aligned parallel to the length of the container (denoted axial strain) and the second aligned parallel to the circumference of the cylinder (denoted hoop strain). Prior to affixing each sensor, a location was

identified where there were no macroscopic scrapes/scratches present as in order to function properly, the sensor must be in intimate contact with the underlying substrate. The container surface was then cleaned using isopropyl alcohol, and an anchor pattern was applied using 240 grit SiC abrasive paper. The anchor pattern itself consisted of a cross-hatched pattern formed by using the abrasive in the lateral direction, followed by the axial direction. Once the anchor pattern was placed, the surface was cleaned again with isopropyl alcohol, after which it was etched using Vishay M-Prep Conditioner-A (a mild phosphoric acid solution). Once etched, the surface was neutralized using Vishay M-Prep Neutralizer 5A (an ammonia based solution). Next, the strain gauge was placed on a segment of Vishay PCT-2M gauge installation tape. The mounting surface of the gauge was then coated with M-Bond 200 adhesion promoter, followed by the M-Bond 200 adhesive (a cyanoacrylate adhesive) and the strain gauge was adhered to the container surface. Once the adhesive cured, leads were soldered to each of the four terminals shown in the figure. The completed gauge was then covered with a urethane coating to protect it from surface damage, and the leads secured to the surface of the container using tape.

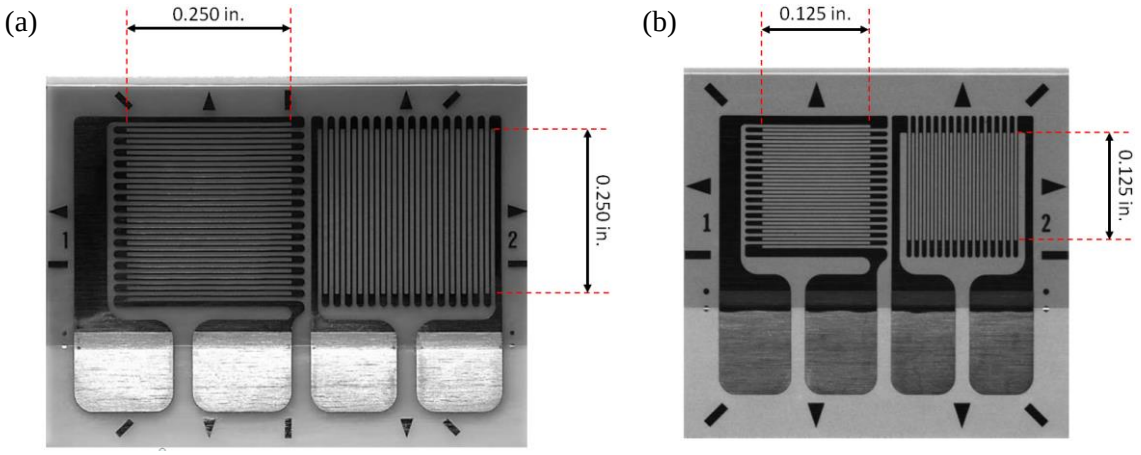

Figure 16: Surface strain gauges used to monitor the strains associated with cutting the mockup container. Most of the sensors were part number CEA-00-250UT-350 (a) along with two smaller CEA-06-125UT-350 (b) strain gauges. Functionally, the two are identical.

Each strain gauge functions as a resistor, with a resistance of 350 ohms. As the surface moves due to stress relaxation, the dimensions of the strain gauge and its resistance also change. Gauges were positioned along both the circumferential and longitudinal welds as illustrated in Figure 17a. In locations where the circumferential weld intersected with a longitudinal weld, three gauges were positioned as illustrated in Figure 17b. Once positioning of the sensors was complete, initial measurements were made to calibrate each of the sensors (Figure 18a). After the initial measurements were made, the container was cut. As one of the sensors was close to the cut region, care was taken to protect that sensor and to prevent coolant splash or tooling damage. Once cutting was complete (Figure 18b), the sensors were monitored again, and the resulting difference in resistance transformed to an equivalent surface strain. In addition to the half of the cylinder reserved for strain analysis, the other half was sectioned into two pieces, as illustrated in Figure 19, for other uses.

(a) (b)

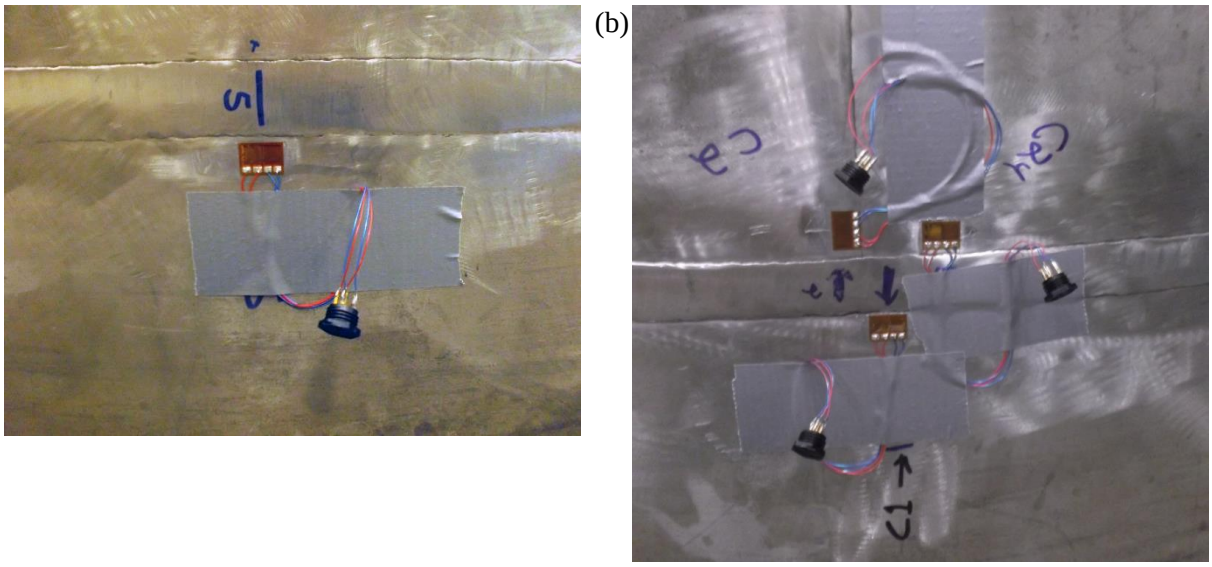

Figure 17: Surface strain gauges were positioned along the longitudinal and circumferential welds. Gauges were placed as close to the weld FZ as possible (a). In addition, a series of three sensors were positioned in each location where a circumferential weld intersected with a longitudinal weld (b).

(a) (b)

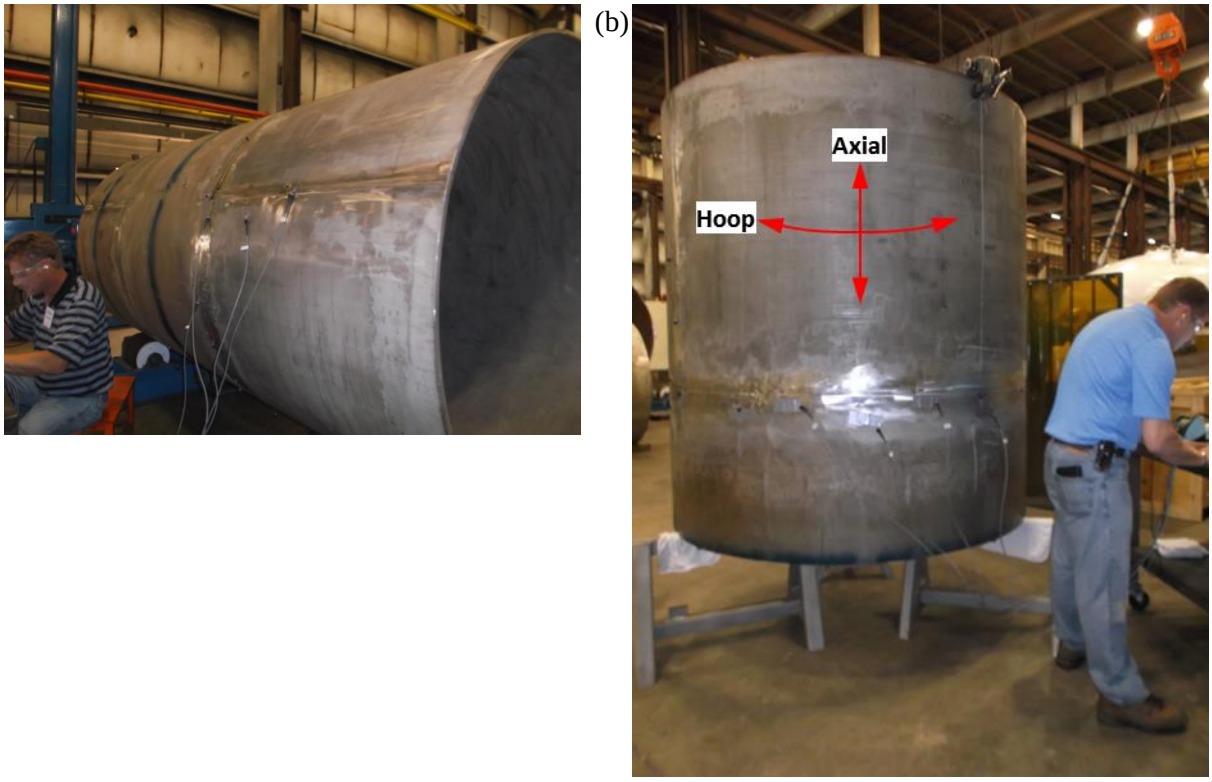

Figure 18: Measurement of strain gauges before (a) and after (b) cutting the container. The data acquisition system enabled four sensors to be monitored at a time, so that they were evaluated in groups. Sensors were measured using the same channel for the initial and final measurements.

(a) (b)

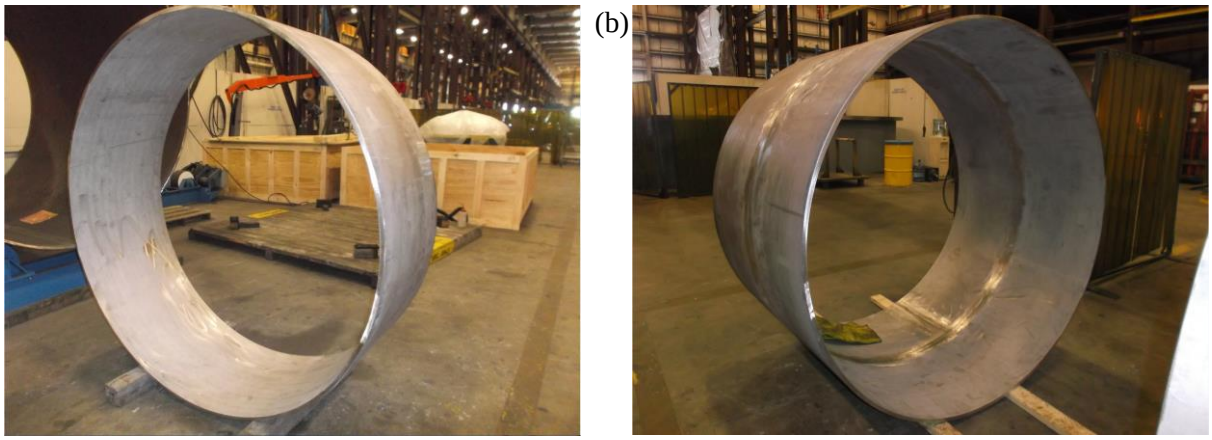

Figure 19: Container was cut into three segments, a 6-foot section used for residual stress analysis; a 2-foot segment for use by EPRI as a small-scale mockup for NDE sensor testing (a); and 4-foot segment for cutting into weld samples for SCC and microstructural characterization (b).

The surface strains measured for the circumferential weld are presented in Figure 20. In terms of their orientation, strains that are parallel with the long dimension of the container are termed "axial strains" and strains that are around the circumference/round dimension of the container are termed "hoop strains". There are two longitudinal welds that intersect with the circumferential weld. The weld which was cut is termed the lower weld, and the uncut weld is termed the upper weld.

The strains along the circumferential weld (Figure 20) were small (microstrain) and primarily tensile in nature, and represent the resolution of the technique as implemented here. At the location where the lower weld (the weld which was cut through) intersected the circumferential weld, the strains were larger, and compressive in the hoop direction (i.e., parallel to the circumference of the container), but remained tensile in the axial direction.

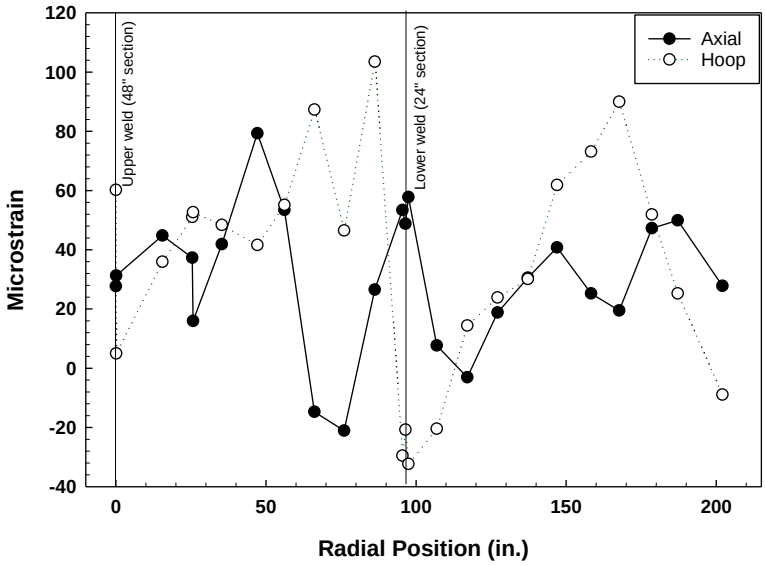

Figure 20: Surface strain measurements along the circumferential weld. Note that the sensors are located approximately 10 inches apart (with exceptions as noted above) and that the overall circumference was 211 inches (i.e., a point at 0" is in the same location as a point at 211").

As discussed previously, sensors were placed alternatively on the upper and lower shell. To evaluate if there was a difference between the strains experienced by the upper and lower shell, the axial (Figure 21a) and longitudinal (Figure 21b) strains were plotted as a function of which shell the respective strain gauge was located. As can be seen in the figure, there is no difference between the two shells (on either side of the circumferential weld).

Measurements were also made along the upper and lower longitudinal welds. The data for the upper weld is illustrated in Figure 22a. As can be seen in the figure, the strains were comparable in magnitude to those around the circumferential welds (i.e., microstrain). Strains were consistently tensile in the axial direction and compressive in the hoop direction. The measurements made at the lower longitudinal weld (Figure 22b) illustrate that significant deformation of the end of the container resulted from the cut. In the longitudinal direction, the strain was tensile, while in the axial direction it was primarily compressive. This indicates that cutting the container in half resulted in a loss of constraint in the regions near the cut. As a result, the stresses from the circumferential weld (tensile hoop stress) resulted in the end of the container becoming smaller in diameter and lengthening slightly. Visually, the container could be considered to be necking down as the location of the cut is approached. Moving further from the cut, the constraint provided by the remaining structure prevented significant surface strain.

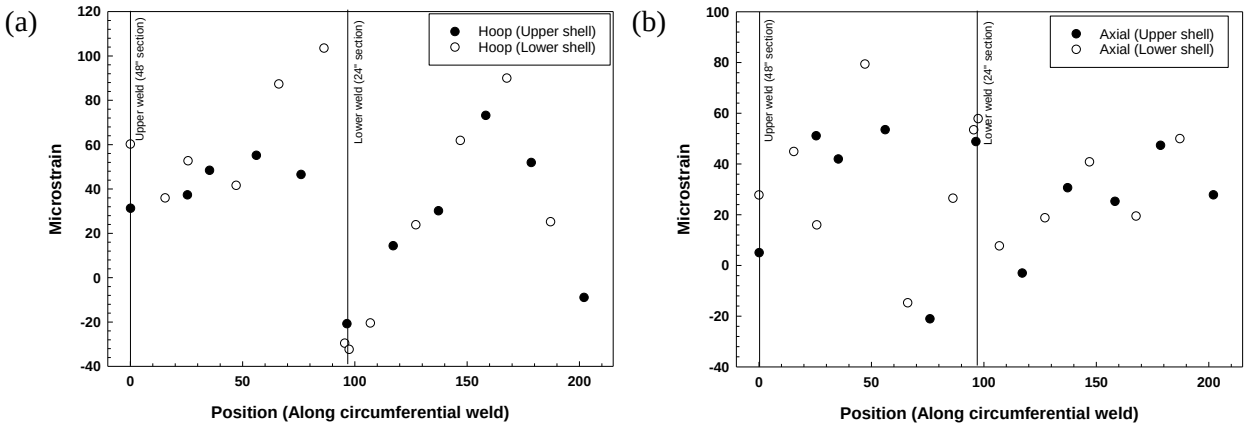

Figure 21: Hoop (a) and Axial (b) strains as a function of position around the circumferential weld, further noted as to which shell the strain gauge was located on.

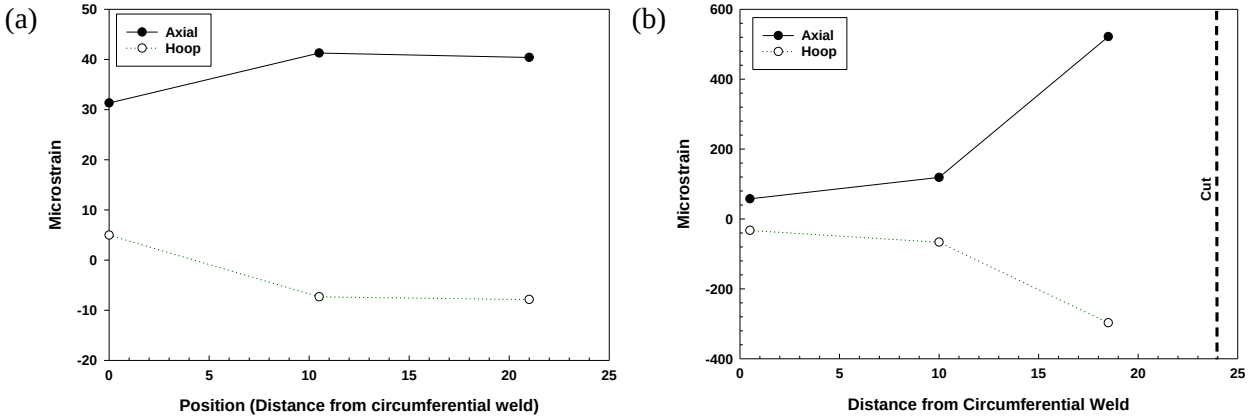

Figure 22: Axial and Hoop strains were measured along the upper (a) and lower (b) longitudinal welds. The lower weld is the one which was cut.

5.2 Residual Stress Measurements

5.2.1 Deep-Hole Drilling Measurements

DHD measurements (and the associated CHD measurements) were performed within the base metal, in the FZ (weld centerline) and HAZ of each weld, as well as in the FZ and HAZ of the weld repair. The data for each measurement is discussed below.

5.2.1.1 Base Metal

The measured ICHD stress distribution for the base metal is shown in Figure 23. As a point of reference, the yield strength of annealed 304L SS is on the order of 170-200 MPa. Very near the surface, the residual stresses were tensile in nature. However, moving into the material, the axial strain remains small and tensile, but the hoop stress becomes compressive in nature. While the data shows a relatively high shear stress in the near surface region, caution must be used when interpreting this result. In order to perform the ICHD measurements in the same location as a subsequent DHD measurement, a very small strain rosette must be used as the diameter of the hole drilled for the ICHD measurement must be smaller than that of the DHD reference hole to prevent the first measurement influencing the second. As a result, the smaller strain gauge samples a smaller effective volume of material, leading to an increased signal–to-noise ratio and a corresponding increased uncertainty. Also, due to the small size of the strain gauges, any misalignment or eccentricity of the drilled hole, i.e. experimental error, is more apparent in the results. The error bars only reflect the magnitude of the uncertainties that can be directly measured, such as curve-fitting error and Young's Modulus uncertainty, and not measurement uncertainty as discussed above. As such, the data in the figure is best interpreted in terms of the average magnitude and trends, and indicates low residual stresses in the first 0.5mm from the OD of the container.

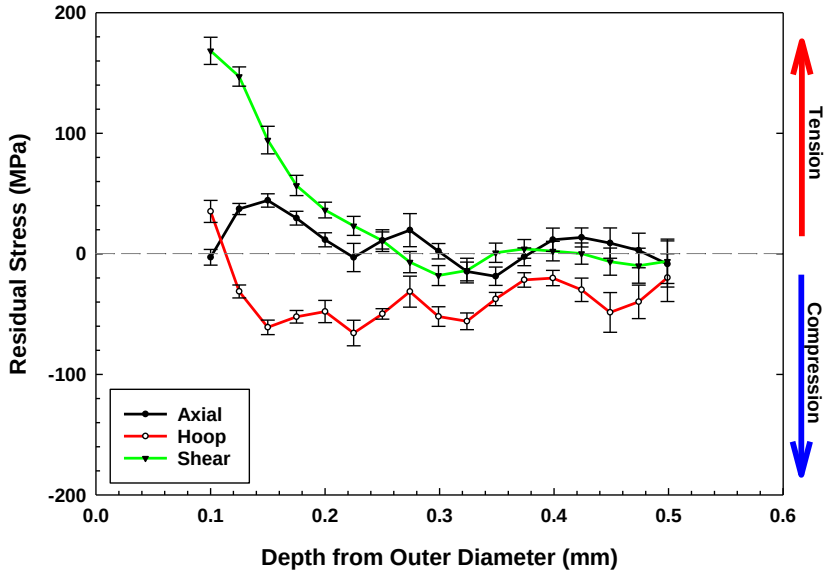

Figure 23: ICHD data for region located for a base-metal region located far from any longitudinal or circumferential weldments.

For the stress distribution through the thickness of the container wall, DHD was performed. In Figure 24, the equipment used to align and stabilize the measurement equipment is shown, along with the directions of each stress that was measured. The region measured is far from the welds, and the anticipated stresses are small relative to the yield strength of the material, so incremental DHD was not necessary.

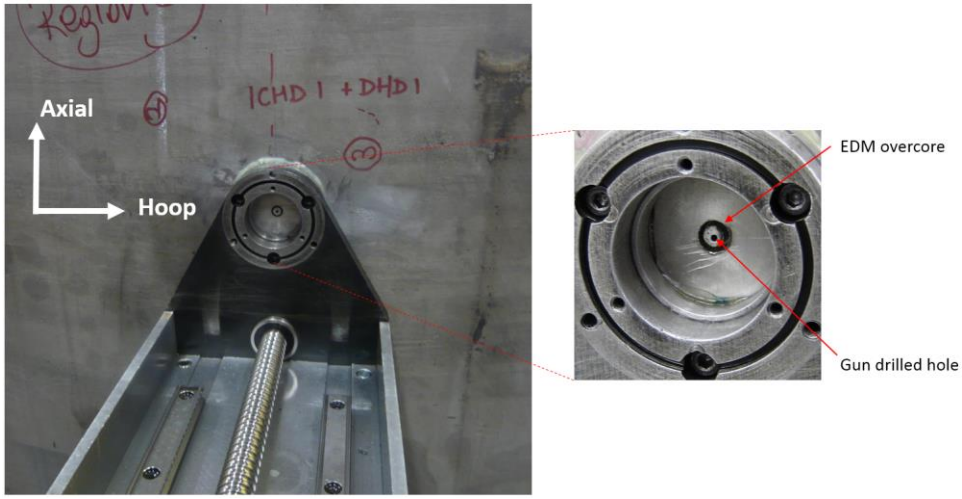

Figure 24: Positioning equipment used to perform DHD measurements of a base metal region (far from any weldments). The orientation of the axial and hoop stresses is indicated on the figure. In the center of the fixture, the hole and EDM over-core can be seen.

The stress distribution through the container wall is shown in Figure 25. Note that data from the near-surface region are not presented in this figure – data for that region were obtained via ICHD and are reported in Figure 23 above. The stress state in the container wall is predominantly tensile in nature in both the axial and hoop directions. Moving further into the wall, the hoop stress becomes increasingly tensile, then both the hoop and axial stresses decrease to approximately zero in the center of the wall. At greater depths from the outer surface, both the hoop and axial stresses then become large and compressive in nature until reaching the inner surface where they again become tensile in nature. The origin of these stresses is illustrated schematically in Figure 26 which shows a flat plate being bent. As the plate is bent, the outer diameter is placed in tension, while the inner diameter is placed in compression. In an ideal case, the stress distribution would show a uniform transition from a maximum tensile stress at the outer diameter to a maximum compressive stress and the inner diameter. However, as the plate is bent, the stresses near the inner and outer diameter become large enough to result in yielding of the material – they do not increase indefinitely. Once the forming stress is released, the resulting stress distribution is as pictured in Figure 25.

The stress profile through the canister shell illustrates why through-thickness cracking is not anticipated at regions away from the weld. While crack initiation can take place at the surface, as the crack grows into the wall, the tensile stresses driving crack propagation will decrease, eventually becoming compressive in nature and arresting crack propagation.

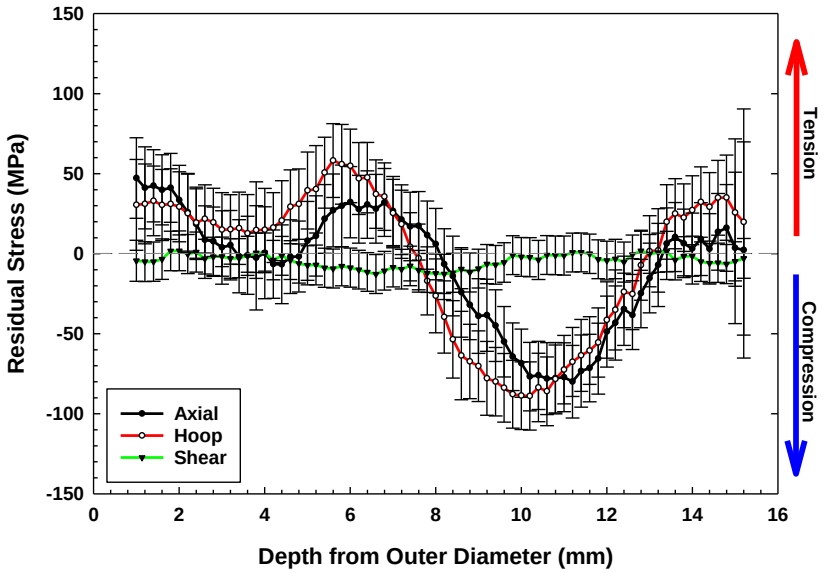

Figure 25: DHD data as a function of distance from the outer diameter of the container for a region located far from any weldments. Note that stresses are tensile near the surfaces, then become compressive in the center of the wall due to the deformation process used to form the original plate material into a cylinder.

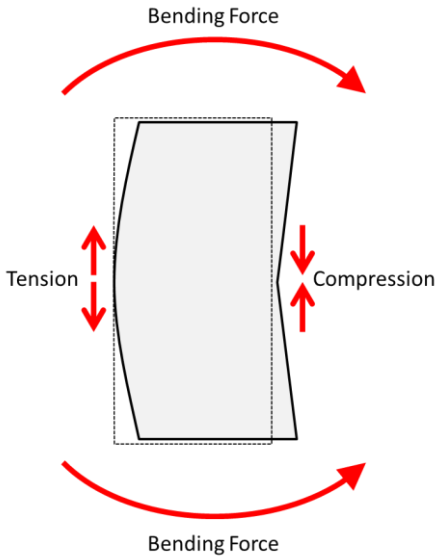

Figure 26: Schematic representation of the forces resulting from bending the plate material used to construct the mockup into a cylinder. Note that this indicates the general forces, and does not capture the near surface deformation resulting from the formation process.

5.2.1.2 Circumferential Welds

As discussed above, the mock storage container has two different types of welds. The welds described in this section are circumferential welds (i.e., the welds that go around the circumference of the mockup container). Due to their orientation, the welds which were anticipated to have the highest residual stresses are the circumferential welds, due to the constraint placed upon them by the surrounding structure. As with the base metal, ICHD was used to measure the near-surface residual stresses, the results of which are shown in Figure 27. In the figure, hoop stresses are parallel to the centerline of the weld (i.e., hoop stresses are parallel to the circumference of the container), and axial stresses are perpendicular to the centerline of the weld (i.e., axial stresses are parallel to the long axis of the cylinder). Both the axial and hoop stresses in the near-surface region are large and tensile in nature, decreasing in magnitude with depth. iDHD was used to measure the residual stresses through the thickness of the weld. In contrast to the base metal, the residual stresses in the weld root are significantly larger in magnitude, and are tensile in nature all of the way through the thickness of the container wall. As a result, if a crack were to initiate at the surface of the container, it would have the driving force necessary to support propagation through the thickness of the wall.

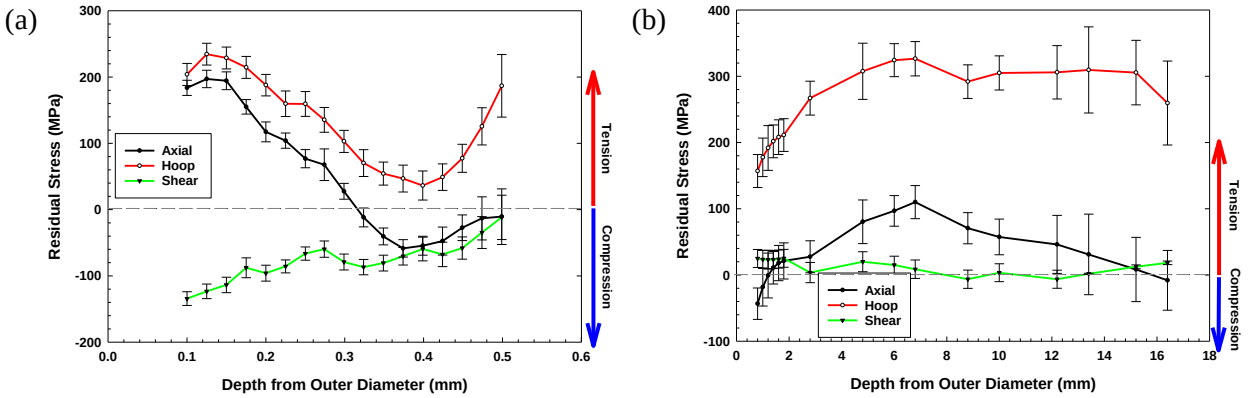

Figure 27: ICHD (a) and iDHD (b) data as a function of distance from the outer diameter of the container for the centerline of a circumferential weld. Note that stresses are tensile through the thickness of the plate, and are largest in magnitude in the hoop direction.

While the residual stresses were anticipated to be largest in the weld FZ, the regions surrounding the weld (the HAZ) are the regions where localized corrosion is most likely to initiate due to sensitization resulting from the thermal profile associated with the welding process. Characterization of the stresses in the HAZ was accomplished by performing ICHD and iDHD measurements approximately 4 mm from the weld toe (i.e., edge of the weld FZ). As with the other two locations, ICHD was used to measure the near-surface residual stresses, the results of which are shown in Figure 28. The hoop stress was large and tensile in nature, increasing in magnitude with depth, while the axial stress in the near-surface region was small and compressive in nature, decreasing in magnitude and eventually becoming tensile in nature with depth. iDHD was used to measure the residual stresses through the thickness of the HAZ. As with the center weld location, the residual stresses in the circumferential weld HAZ are tensile through the entire thickness of the shell, potentially capable of supporting through-thickness crack propagation.

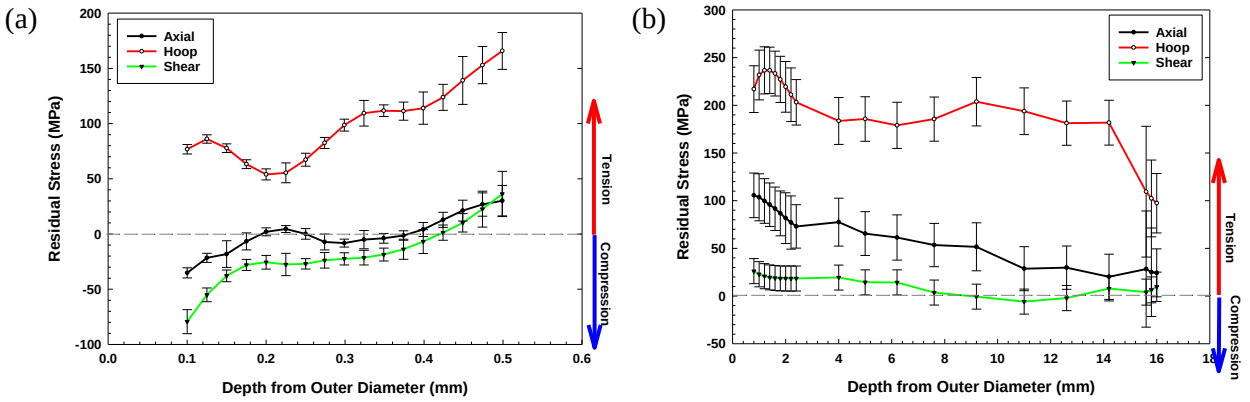

Figure 28: ICHD (a) and iDHD (b) data as a function of distance from the outer diameter of the container for the HAZ associated with a circumferential weld. Measurements were made approximately 4mm from the weld toe. Note that stresses are tensile through the thickness of the plate, and are largest in magnitude in the hoop direction.

5.2.1.3 Longitudinal Welds

The welds described in this section are longitudinal welds (i.e., the welds that are parallel to the long axis of the mockup container). As with the other DHD and iDHD measurements, ICHD was used to measure the near-surface residual stresses, the results of which are shown in Figure 29. In the figure, hoop stresses are perpendicular to the centerline of the weld (i.e., hoop stresses are parallel to the circumference of the container), and axial stresses are parallel to the centerline of the weld (i.e., axial stresses are parallel to the long axis of the cylinder). The axial stress in the near surface region was large and tensile in nature, decreasing in magnitude with depth, while the hoop stress was large and compressive in nature near the surface, decreasing and eventually becoming tensile with depth. iDHD was used to measure the residual stresses through the thickness of the weld. As with the circumferential weld, the stresses both parallel and perpendicular to the weld centerline are strongly tensile in nature, and at no point do they become compressive. As a result, if a crack were to initiate at the surface of the container in the longitudinal weld centerline, it would have a tensile stress available to support propagation through the thickness of the wall.

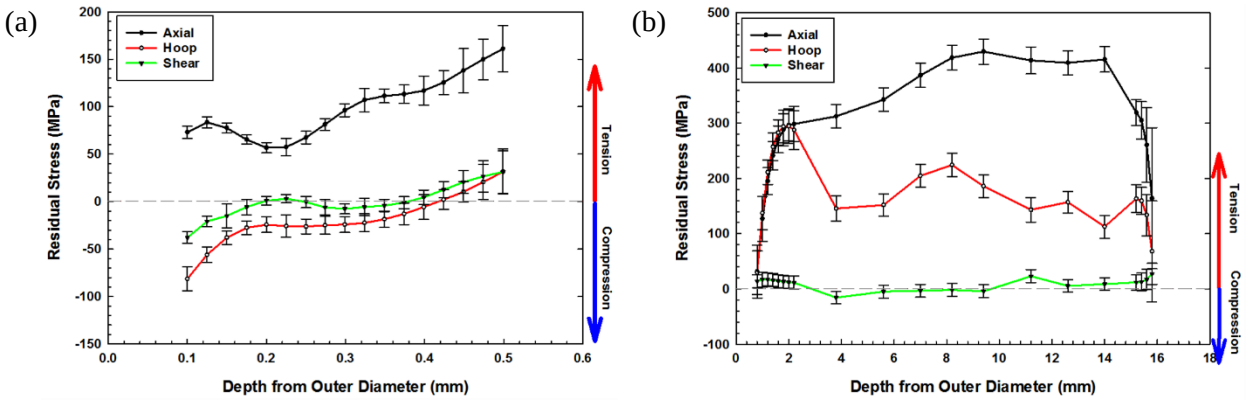

Figure 29: ICHD (a) and iDHD (b) data as a function of distance from the outer diameter of the container for the centerline of a longitudinal weld. Note that because the weld is aligned parallel to the long axis of the container, axial stresses are now parallel to the weld centerline.

While the residual stresses are largest in the weld fusion zone, the HAZ surrounding the weld is the regions where localized corrosion is most likely to initiate due to sensitization resulting from the thermal profile associated with the welding process. As with the circumferential weld, characterization of the stresses in the HAZ was accomplished by performing ICHD and iDHD measurements approximately 4 mm from the weld toe (i.e., edge of the weld fusion zone). As with the other locations, ICHD was used to measure the near-surface residual stresses, the results of which are shown in Figure 30. Both the axial and hoop stresses in the near surface region are large and tensile in nature, decreasing in magnitude with depth. iDHD was used to measure the residual stresses through the thickness of the weld. As with the circumferential weld HAZ, through-wall tensile stresses are present, and could support crack propagation through the thickness of the wall.

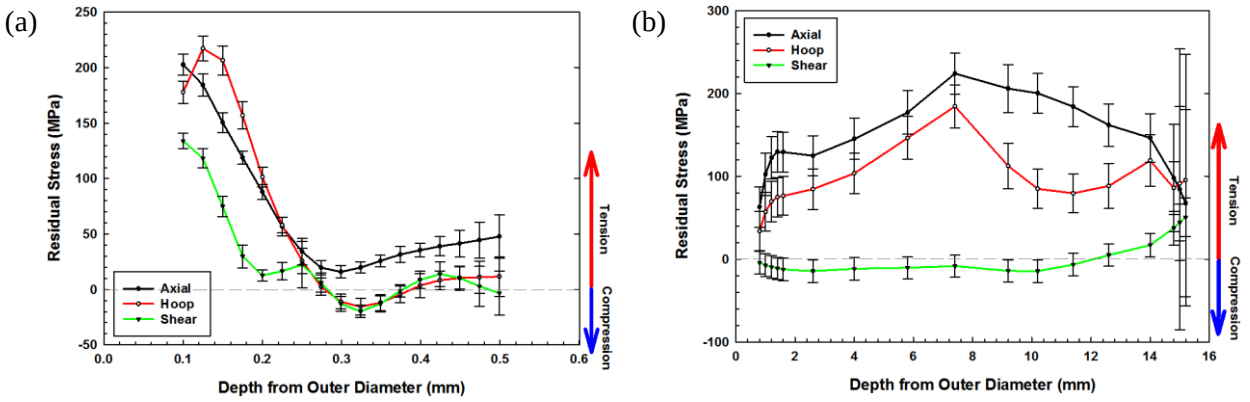

Figure 30: ICHD (a) and iDHD (b) data as a function of distance from the outer diameter of the container for the HAZ of a longitudinal weld. Note that stresses are tensile through the thickness of the plate, and are largest in magnitude in the axial direction.

5.2.1.4 Circumferential Weld Repair

As discussed previously, it is not uncommon for the welds on an interim storage container to have been repaired during the production process (i.e., portions of the weld that are out of compliance with the standards are ground out and the area re-welded). These repair regions have been identified by numerous researchers as having dramatically elevated residual stresses when compared to unrepaired portions of a weld (Dong et al., 2002, Bouchard et al., 2005, Dong et al., 2005, Elcoate et al., 2005, George and Smith, 2005, Hossain et al., 2006, Hossain et al., 2011). No weld defects requiring repair were identified following production. However, because of the impact weld repairs can have on the residual stresses in adjacent material, a repair of a simulated defect was made on each circumferential weld. In these locations, an artificial defect corresponding to a 1/8" diameter hole was drilled partially into the outer diameter, simulating a small defect such as porosity or an entrained slag particle (illustrated schematically in Figure 6). The "defect" was then removed by machining out a larger region via a ¼" drill, after which the edges of the drilled out region were ground to a bevel, such that it could be re-welded.

The repair region was evaluated in the same manner as the unmodified circumferential and longitudinal welds. ICHD and iDHD measurements were made in the center of the repair, as well as in the HAZ. As discussed in Section 3, there is an apparent misalignment of the ID and OD welds as presented in Section 3 (see Figure 4)., the HAZ was evaluated on both sides of the weld repair. To make sure that possible asymmetries in the stress field were captured, a measurement was made in the HAZ of both sides of the repair. Cross sectional evaluation of the welds, combined with the full volumetric inspection performed when the mock-up was manufactured indicate that this misalignment was, in fact, due to the final weld passes for the OD weld being asymmetric. The degree of misalignment between the ID and OD welds is illustrated in Figure 31below, and should be considered when evaluating the stress profiles collected. For

instance, the weld repair, centered in the outer weld, is actually near the lower edge of the inner weld. Moreover, the upper and lower HAZ measurements are equally spaced above and below the outer weld, but not the inner weld.

The stress distribution for the center of the weld repair is presented in Figure 32. As with the unrepaired regions, the stress is strongly tensile in both the hoop and axial directions. The stress distribution is symmetric – being comparable in magnitude in both of these directions, particularly near the weld surface. This symmetry is consistent with the nature of the weld repair, which was circular in nature. Though the repair was located on the OD, the amplification in the stress state was present completely through the thickness of the weld. This is consistent with what has been observed by other researchers on linear weld repairs in pipes and similar structures.

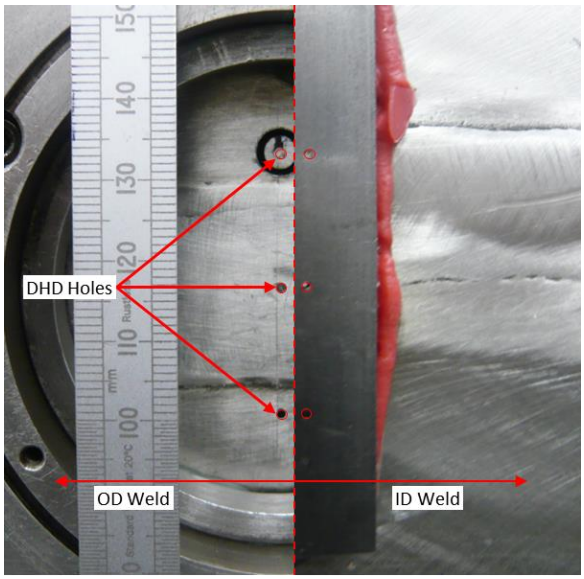

Figure 31: iDHD holes associated with the weld repair. OD is on the left and ID on the right. The holes suggested significant misalignment, though weld cross sections indicate that the final pass on the OD weld is likely causing the perceived asymmetry.

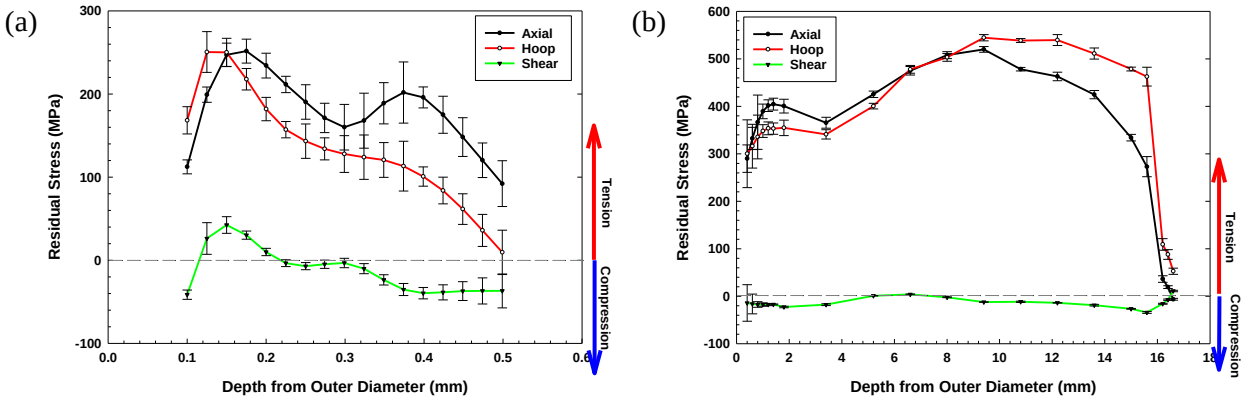

Figure 32: ICHD (a) and iDHD (b) data as a function of distance from the outer diameter of the container for the center of the repaired region in the circumferential weld. Note that stresses are tensile through the thickness of the plate, and are comparable in magnitude in the hoop and axial directions, consistent with the symmetric nature of the repair.

While the residual stresses are largest in the weld FZ, the HAZ is the region where localized corrosion is most likely to initiate due to sensitization resulting from the thermal profile associated with the welding process.

The residual stress data for the uppermost HAZ measurement pictured in Figure 31 is presented in Figure 33. As with the other measurement locations, the near-surface stresses were evaluated using ICHD, followed by the iDHD measurement. As with the center of the repair, both the axial and hoop stress components were strongly tensile in nature. However, while the center of the weld had a symmetric stress distribution, for the HAZ, the axial portion (i.e., stresses perpendicular to the centerline of the weld) were substantially larger in magnitude at the surface, becoming comparable in magnitude as the inner diameter surface was approached. The second HAZ measurement (the lowermost hole in Figure 31) is shown in Figure 34. Similar to the upper measurement, both the axial and hoop stresses are strongly tensile in nature, with the axial stress being the larger of the two. As the inner wall is approached, the axial and hoop stresses become comparable.

A comparison of the stresses measured in the repair region with those of an unrepaired region of the circumferential weld is presented in Figure 35. In the case of the weld centerline/center of the repair region, the stresses are substantially amplified in the repaired region, though the shape of the distribution is largely maintained. In the case of the HAZ, however, while the axial stress is substantially increased by the weld repair, the hoop stress remained closer to that observed in an unrepaired region. The amplification of the axial stress in the HAZ is particularly important as this stress is perpendicular to the weld centerline – though the residual stress is only part of what drives crack direction, a dominant axial tensile stress would tend to support cracks that are parallel to the circumferential weld, rather than perpendicular to it.

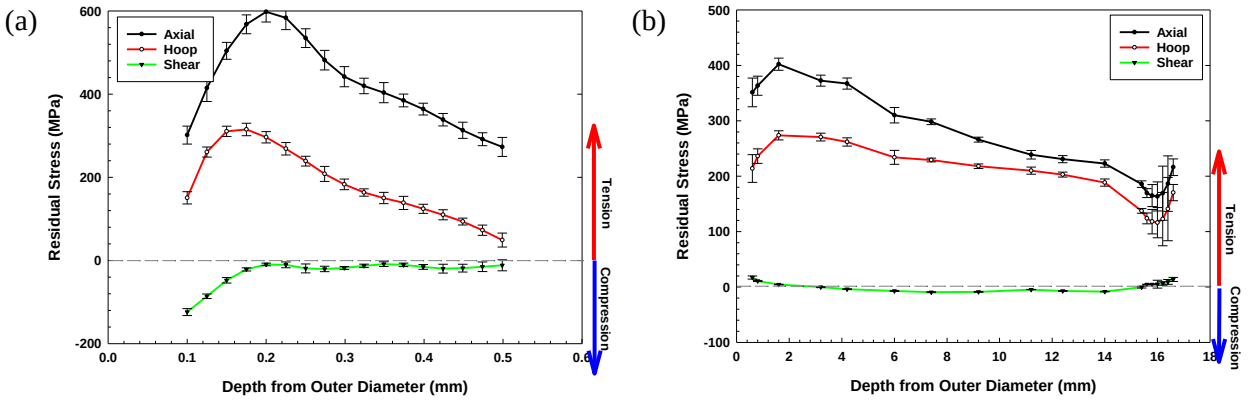

Figure 33: ICHD (a) and iDHD (b) data as a function of distance from the outer diameter of the container for the HAZ associated with the repair of the circumferential weld (upper location in Figure 31). Note that stresses are tensile through the thickness of the plate, and are largest in magnitude in the axial direction.

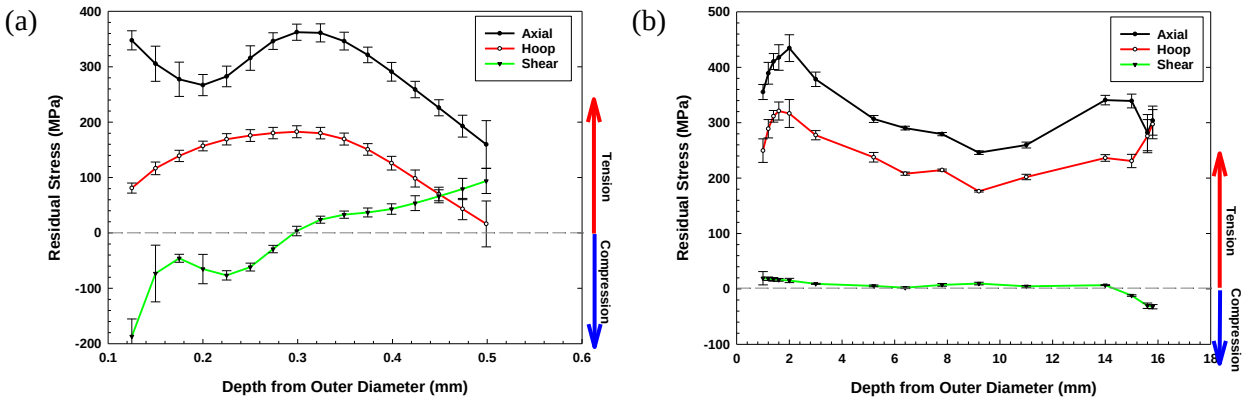

Figure 34: ICHD (a) and iDHD (b) data as a function of distance from the outer diameter of the container for the HAZ associated with the repair of the circumferential weld (lower location in Figure 31). Note that stresses are tensile through the thickness of the plate, and are largest in magnitude in the axial direction.

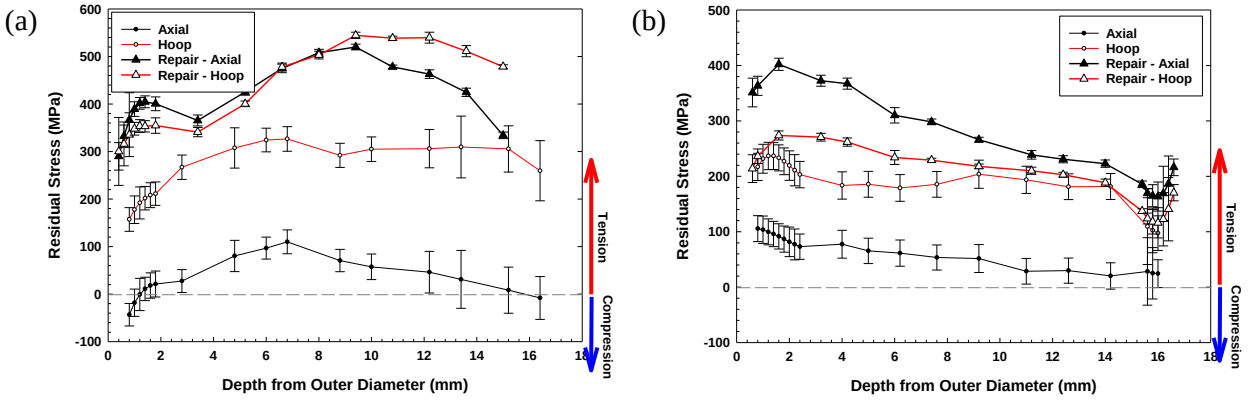

Figure 35: Comparison of the residual stresses as measured via iDHD for the circumferential weld centerline (a) and HAZ (b) to those measured for the repaired region in the center of the repair and associated HAZ.

5.2.2 Contour Method

As discussed previously, the contour method is similar to the DHD and iDHD techniques in that displacements due to stress relaxation are measured at a cut surface, then converted to a pre-existing residual stress. As with DHD, the results can be influenced by plasticity effects due to high levels of residual stress. Unlike the DHD technique, where the stress is measured at a single location through the thickness of the wall, the contour method gives a map of the entire cross section. Contour measurements were made across the longitudinal and circumferential welds, as well as through a weld intersection. Comparisons have been made to the DHD measurements that were made through the same region. While such comparisons can be made, some deviations are to be expected due to heterogeneities which may exist in the weld along its length (e.g., weld pass start/stop locations, etc.).

5.2.2.1 Circumferential Weld Contour Data

A map of the hoop stress as a function of position in the form of both a surface plot and a contour plot for the circumferential weld is presented in Figure 36. As can be seen in the figure, the residual stress is strongly tensile through thickness near the weld centerline, extending approximately 50 mm away from the center of the FZ. Further from the weld centerline, the stress state begins to approach that of the base metal. Note that, on this map and on others presented here, the tensile zones to the far left and right, at the edges of the sample where the raw data and models are less well defined, are exaggerated by the analysis process. Care must be taken when interpreting the contour results in these regions.

The measured stresses show a strong banding perpendicular to the canister wall. On the contour maps for the circumferential weld and the weld intersection regions, a strong vertical banding is visible. This indicates variations in the hoop residual stresses created by bending the plates. The banding is not visible in the seam weld contour map, because axial residual stresses were measured and were unaffected by the bending.

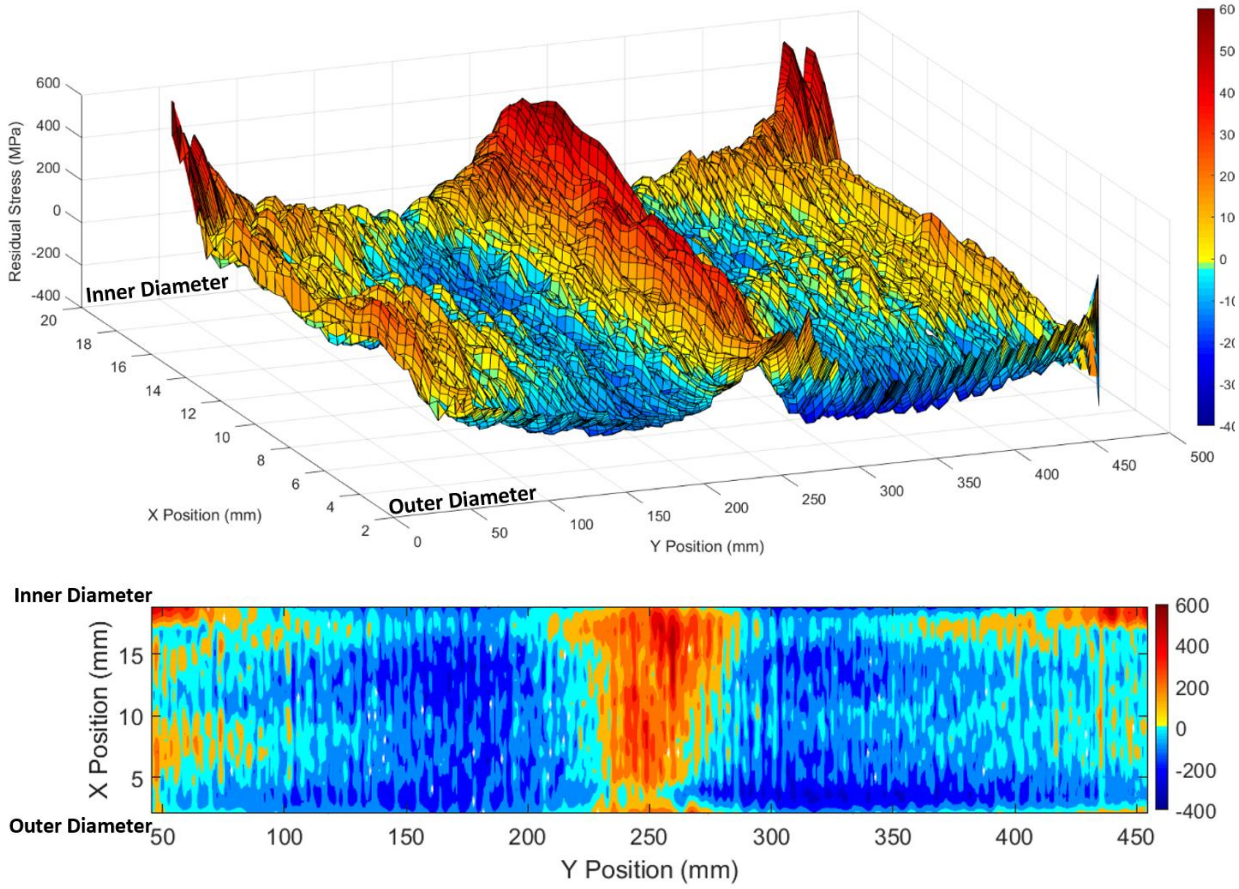

Figure 36: Contour map across a circumferential weld. Primary stress illustrated is the hoop stress (parallel to the weld direction). The cross section is 400 mm in length, and centered around the weld centerline. Red, yellow, and green represent tensile stresses, while blue represents compressive stresses. The through-wall tensile stress field extends approximately 50mm from the weld centerline.

Deep hole drilling measurements were made in the FZ and HAZ of the circumferential weld, shown in Figure 27 and Figure 28, respectively. Comparison of the contour data at those locations is presented in Figure 37. In the case of the weld centerline (Figure 37a), the data (a slice taken at a position of 249mm in Figure 36) is in good agreement in terms of the magnitude. The stress is strongly tensile through the entire thickness of the container wall in the hoop direction. In the HAZ (Figure 37b), taken at a position of 268mm in Figure 36, the magnitude is comparable, but the stress does appear to go slightly compressive approximately 4mm into the container wall. There are a number of explanations for this apparent difference. The primary difference between the two techniques is that while the DHD measurements were made with the intact structure, the contour measurements were made after the container had been sectioned and as such, the stress due to the constraint of the structure had been relaxed. This is demonstrated in Figure 38, which illustrates the spring back of the container as it was sectioned (i.e., the bending stress that was relaxed when the cylinder was cut has not been added back into the data in the figure). In addition, looking at the contour, it is apparent that the stress distribution is complex – as you pass further from the weld centerline, local regions of compression become visible. In addition, as discussed in Section 3, the weld was somewhat asymmetric in appearance when referencing from the outer diameter. As such, exact positioning of the deep hole drilling measurement relative the actual centerline of the weld won't be known until the container has been cross sectioned at those specific locations. At the time this report is being written, the container has not yet been returned from the stress analysis vendor, so such measurements have not yet been made. Finally, looking at the contour and moving away from the weld centerline (in either direction), there are regions where the stress transitions to a compressive value, then transitions back to a tensile value. As DHD is a point measurement, it cannot capture these three dimensional fluctuations.

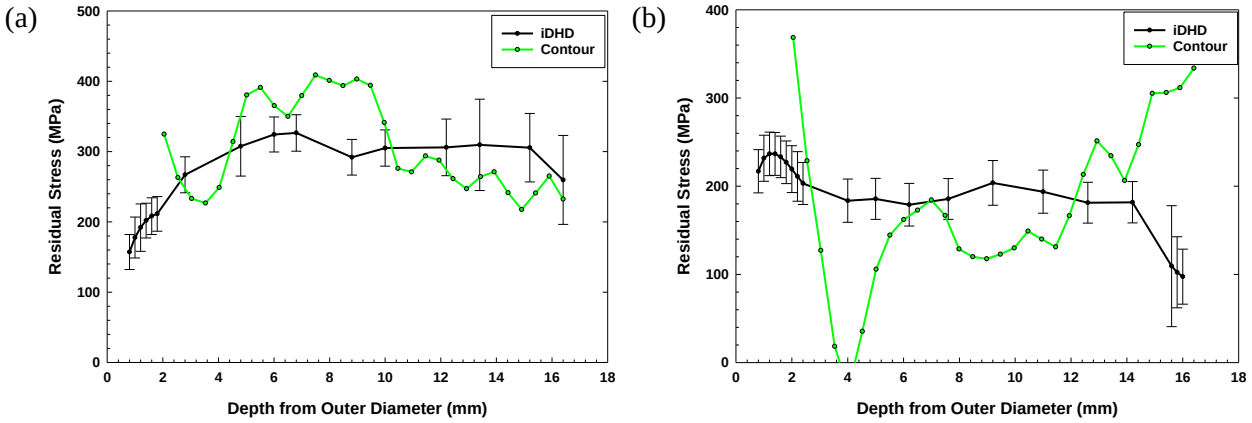

Figure 37: Comparison of the contour data for the hoop stress measured via the deep hole drilling technique for the (a) weld centerline and (b) HAZ.

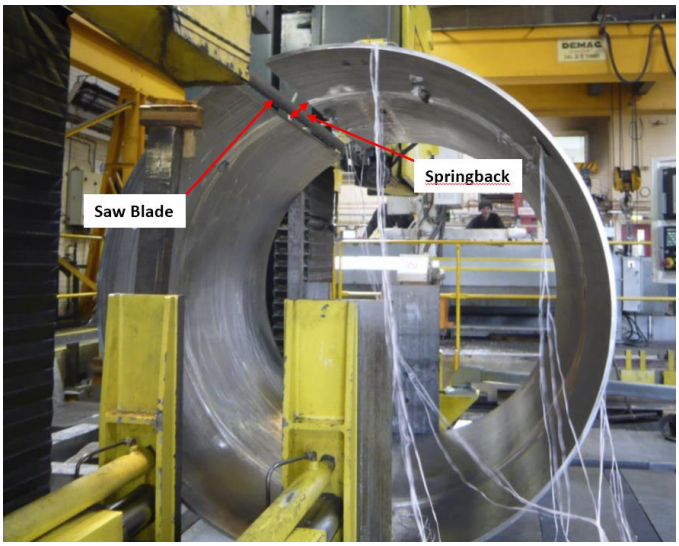

Figure 38: Initial sectioning of the mockup using a band saw. Upon making the axial cut, there was significant spring-back of the container as the constraint imposed by the cylindrical structure was removed.

5.2.2.2 Longitudinal Weld Contour Data

A map of the axial stress as a function of position for the longitudinal weld in the form of both a surface plot and a contour plot is presented in Figure 39. As can be seen in the figure, the residual stress is strongly tensile through thickness near the weld centerline, extending approximately 25 mm away from the center of the FZ. Further from the weld centerline, the stress state begins to approach that of the base metal. While the stress does become compressive, there remain regions that are tensile in nature, extending well into, and in some cases, completely through the container wall. As was indicated in the discussion of the deep hole drilling data, the stress levels were higher in regions near the weld. This is also apparent in the contour, however, while the peak stresses are higher than those found for the circumferential weld, the width of the stress field is smaller.

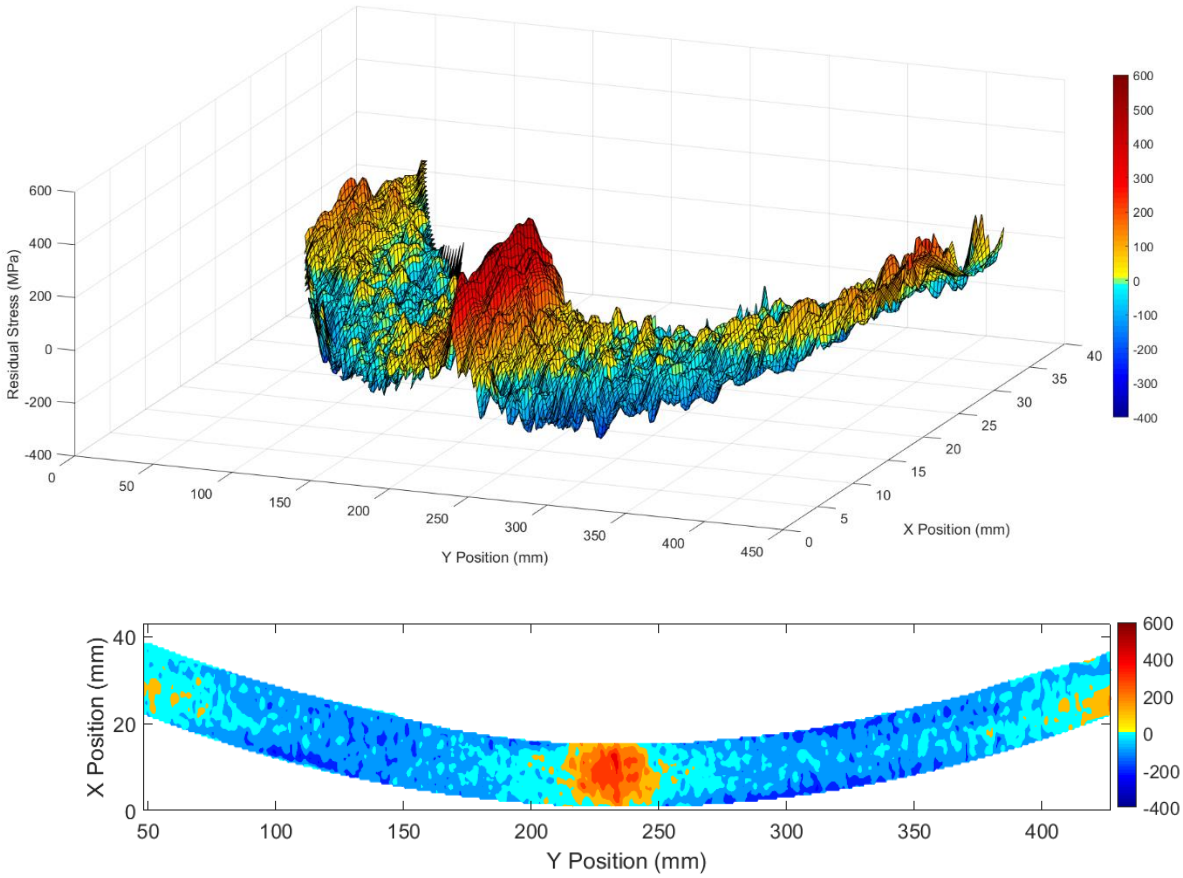

Figure 39: Contour map across a Longitudinal weld. Primary stress illustrated is the axial stress (parallel to the weld direction). The cross section is 400mm in length, and centered around the weld centerline. Red and yellow represent tensile stresses, while green and blue represent compressive stresses. The through-wall tensile stress field extends approximately 25mm from the weld centerline.

Deep hole drilling measurements were made in the FZ and HAZ of the longitudinal weld, shown in Figure 29 and Figure 30, respectively. Comparison of the contour data at those locations is presented in Figure 40. In the case of the weld centerline (Figure 40a), the data (taken as a slice at a position of 233mm in Figure 39) is in good agreement in terms of the magnitude and shape of the distribution. The stress is strongly tensile through the entire thickness of the container wall in the hoop direction. In the HAZ (Figure 40b), the data was taken at a position of 215mm in Figure 39, and while magnitude is

comparable, but the stress becomes markedly less tensile at the outer diameter, but then matches the distribution well towards the inner diameter of the container wall. This deviation is similar to that observed for the hoop stress in the longitudinal weld, and again, there are a number of explanations for this apparent difference. First, as stated above for the circumferential weld, the contour measurement is made after sectioning the container, and as such the stress state will change due to relaxation due to the removal of constraint (i.e., the bending stress that was relaxed when the cylinder was cut has not been added back into the data in the figure). Furthermore, looking at the contour, it is apparent that the stress distribution is complex – as you pass further from the weld centerline, local regions of compression become visible. In addition, as discussed in Section 3, the weld was somewhat asymmetric in appearance when referencing from the outer diameter. As such, exact positioning of the deep hole drilling measurement relative the actual centerline of the weld won't be known until the container has been cross sectioned at those specific locations. At the time this report is being written, the container has not yet been returned from the stress analysis vendor, so such measurements have not yet been made. Finally, looking at the contour, there are variations in the stress, particularly looking further from the weld centerline. These would not be captured in the deep hole drilling measurement, but can be seen here.

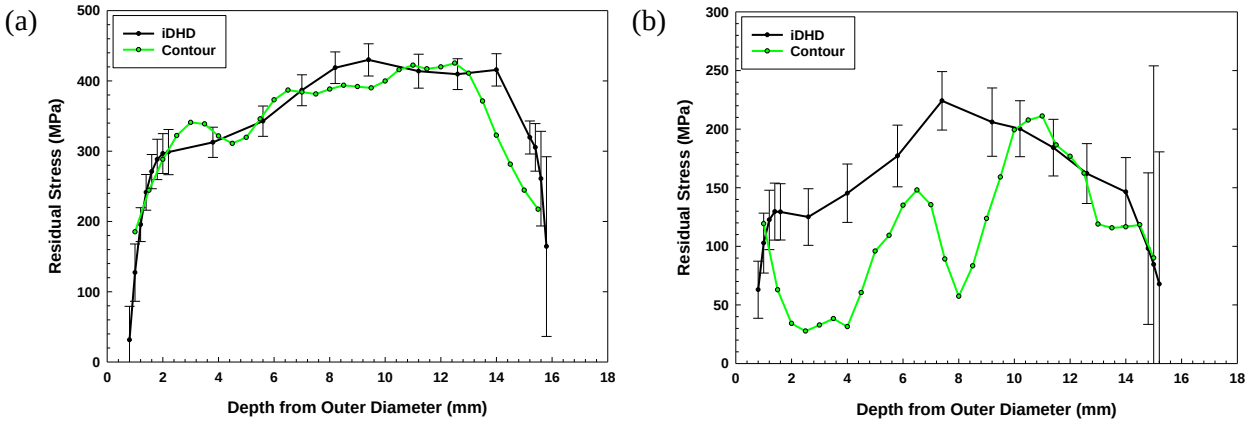

Figure 40: Comparison of the contour data for the axial stress measured via the deep hole drilling technique at a longitudinal weld for the (a) weld centerline and (b) HAZ.

5.2.2.3 Weld Intersection Contour Data

A final contour measurement was made at the intersection of a circumferential weld with a longitudinal weld, shown in the form of both a surface plot and a contour plot in Figure 41. As seen in the figure, the distribution is markedly different than the cross section through the circumferential weld presented in Figure 36. While the magnitude appears similar, the stress field extends further from the FZ centerline, and appears to be biased towards the inner diameter of the container. In addition, the hoop stress in the longitudinal weld centerline has become compressive, unlike the tensile stress field illustrated for regions far from the weld intersection, and illustrated via iDHD in Figure 29.

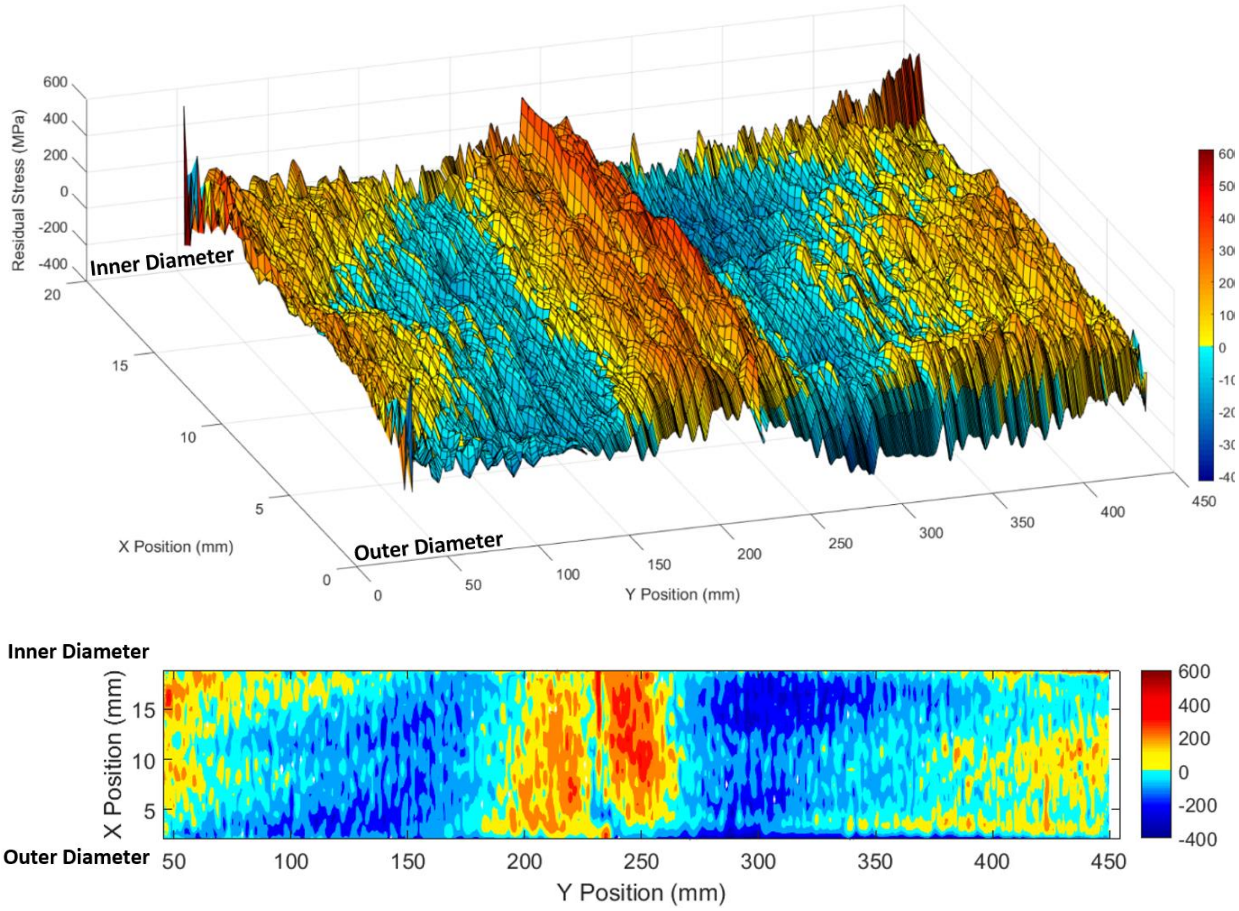

Figure 41: Contour measurement through the intersection of a longitudinal weld with a circumferential weld. The contour is centered on the circumferential weld, with the longitudinal weld being to the right, and the lower container shell to the left.

5.2.3 X-Ray Diffraction

X-ray diffraction was used to assess the residual stress associated with the base metal, the circumferential welds, and the intersection of a circumferential weld with a longitudinal weld. Due to the low penetration depth of x-rays into the metal being evaluated, only the very near surface stresses can be measured (i.e., tens of microns into the sample) – much closer to the surface than any of the other techniques used here are capable of.

The application of the technique to the circumferential weld, and the resulting stress distribution, is illustrated in Figure 42. The technique was unsuccessful at obtaining the residual stress state on the weld itself (i.e., the weld FZ) due to a combination of the microstructure and surface topography in that region,

but was able to obtain data in the HAZ moving away from the weld. As shown in the figure, the measured stresses are strongly compressive in the HAZ adjacent to the weld FZ, but become tensile beyond approximately 100mm from the weld centerline. The magnitudes of the axial and hoop stresses are comparable to one another, though the hoop stress appears to approach the stress associated with the base metal more rapidly than the axial stress. The presence of a strong compressive stress is in stark contrast to the ICHD data which shows a predominantly tensile stress in the hoop direction, and slightly compressive in the axial direction for the HAZ associated with the circumferential weld, and strongly tensile in both the axial and hoop directions for the HAZ associated with the longitudinal weld or with the weld repair region in the circumferential weld. The reason for this discrepancy is likely due to the very shallow depth that the XRD technique is able to sample, coupled with the surface condition of the mockup container welds. As illustrated in Figure 5, the weld bead and the region surrounding the weld has been ground. This mechanical deformation can significantly alter the stress state and plastic strain experienced by the material, as discussed by Ghosh, et al. 2010.

(a) (b)

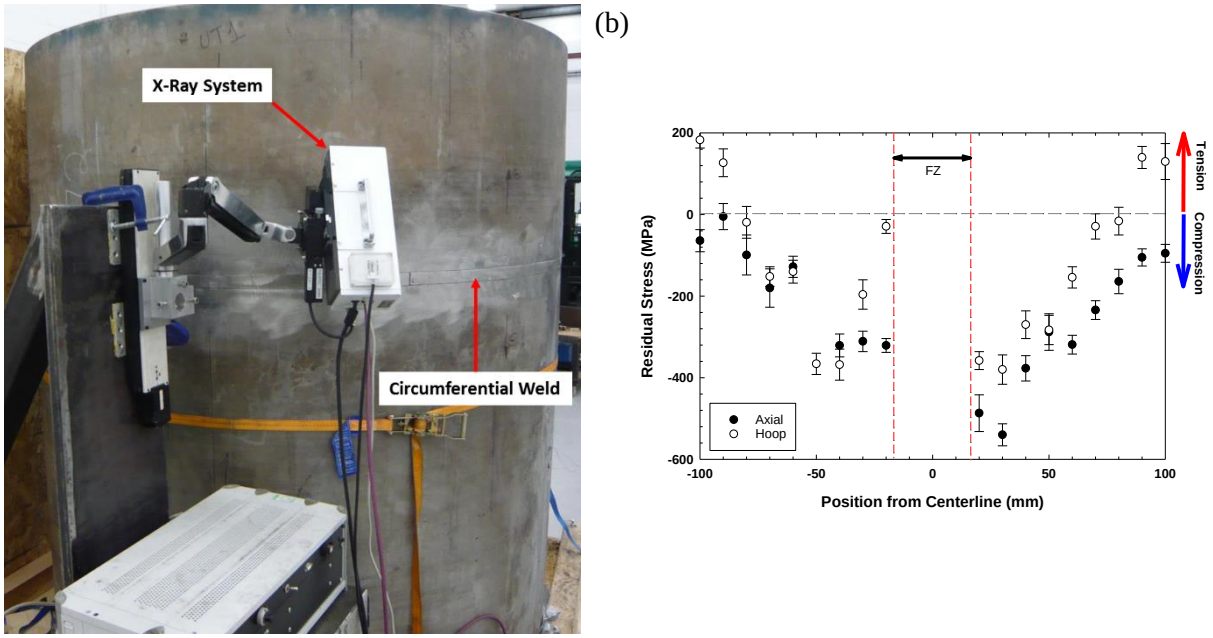

Figure 42: XRD evaluation of a circumferential weld showing (a) the equipment configuration, and (b) the resulting stress distributions.

Near-surface residual stresses were also evaluated for the intersection of a longitudinal weld with a circumferential weld (Figure 43a). As with the circumferential weld, the XRD technique was not able to discern the stress state in the weld FZ, and only the stresses in the HAZ as a function of distance from the centerline of the circumferential weld were measured. The stresses are compressive in nature, with the magnitude decreasing with distance from the weld intersection point. The compressive residual stress is, again, likely the effect of the surface grinding which was done on the surface of the weld FZ, as well as the metal adjacent to it. Finally, the surface stress in the base metal, far from a weld, was assessed (Figure 43b). In this case, while the axial stresses were compressive, the hoop stress was tensile in nature.

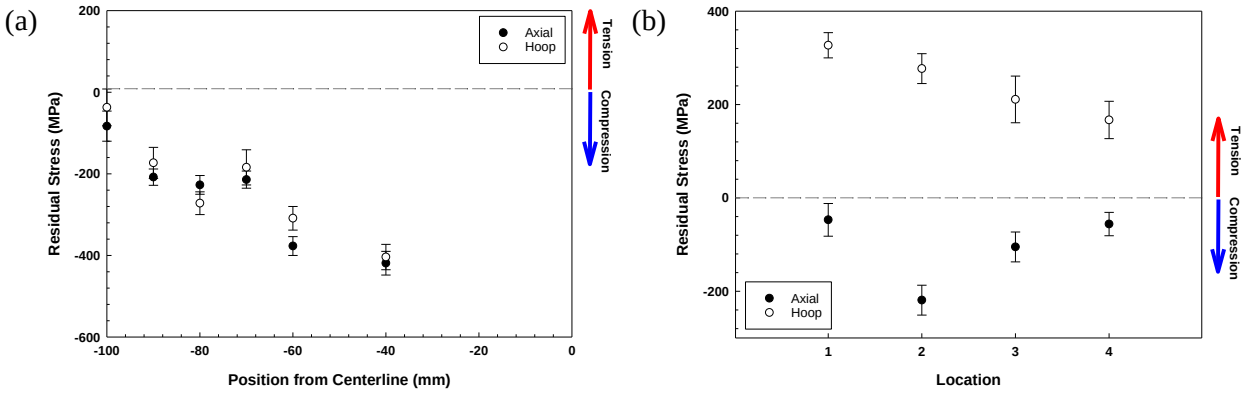

Figure 43: XRD evaluation of the near surface residual stresses associated with (a) the intersection of a circumferential weld and longitudinal weld, and (b) within the base metal far from any welds. For the intersection of the two welds, the position is noted as the distance from the centerline of the circumferential weld into the un-welded container wall, in the same orientation as the longitudinal weld.

5.2.4 Ultrasonic Measurement

Ultrasonic measurements were conducted in three locations: across a longitudinal weld, across a circumferential weld, and across the intersection of a longitudinal weld with a circumferential weld (passing along the centerline of the longitudinal weld, across the circumferential weld and into the base metal). The resulting data from each ultrasonic measurement location is compared to similar measurements made via the contour and hole drilling techniques discussed above in Figure 44. Note that for the contour and DHD measurements in that figure, the data has been averaged over the same gauge length as the ultrasonic measurement. The impact of not averaging is illustrated in Figure 45 for a circumferential weld (at a depth of 2.8mm), illustrating how the averaging results in the inability of the ultrasonic technique to resolve locally high stresses captured by the contour measurement.

In contrast to the other techniques, values obtained through ultrasonic measurements are indicative of the stress state within a volume of material. As such, they are effectively averaged, and were anticipated to yield a smoother response with significantly reduced point to point irregularities/noise. The accuracy of the measurement is a function of the parameters derived to describe the acousto-elastic property of the material. In this study, while two separate locations (one in the base metal, and one in the weld fusion zone, with replicates of each location used) were used, a single value was determined and assumed to be applicable in all locations. As the parameters used to describe the acousto-elastic properties of a material are also a function of microstructure, it is anticipated that the use of a single value for all locations will result in some inaccuracies. Nevertheless, as a proof of concept experiment, the resulting inaccuracy is acceptable.

In Figure 44, it can be seen that the peak stress at the primary weld centerline for each ultrasonic measurement location was comparable. The difference seen both by deep hole drilling and the contour measurement method was not observed. Aside from that, the shape and relative magnitude of the stresses reported from the ultrasonic measurements were comparable to those obtained via other techniques. As such, it appears that the ultrasonic measurement technique offers great promise as a non-destructive stress measurement method, with the potential to offer a precision comparable to other techniques that, while they yield a more complete map (e.g., contour measurement or deep hole drilling), are destructive in nature and as such may not be used in many applications. As an example, an immediate application for this technique would be to evaluate new storage containers for repair regions that result in an unacceptably high residual stress state. This would allow the end user to then either reject the container, or apply a stress mitigation method to the region with a highly elevated stress state.

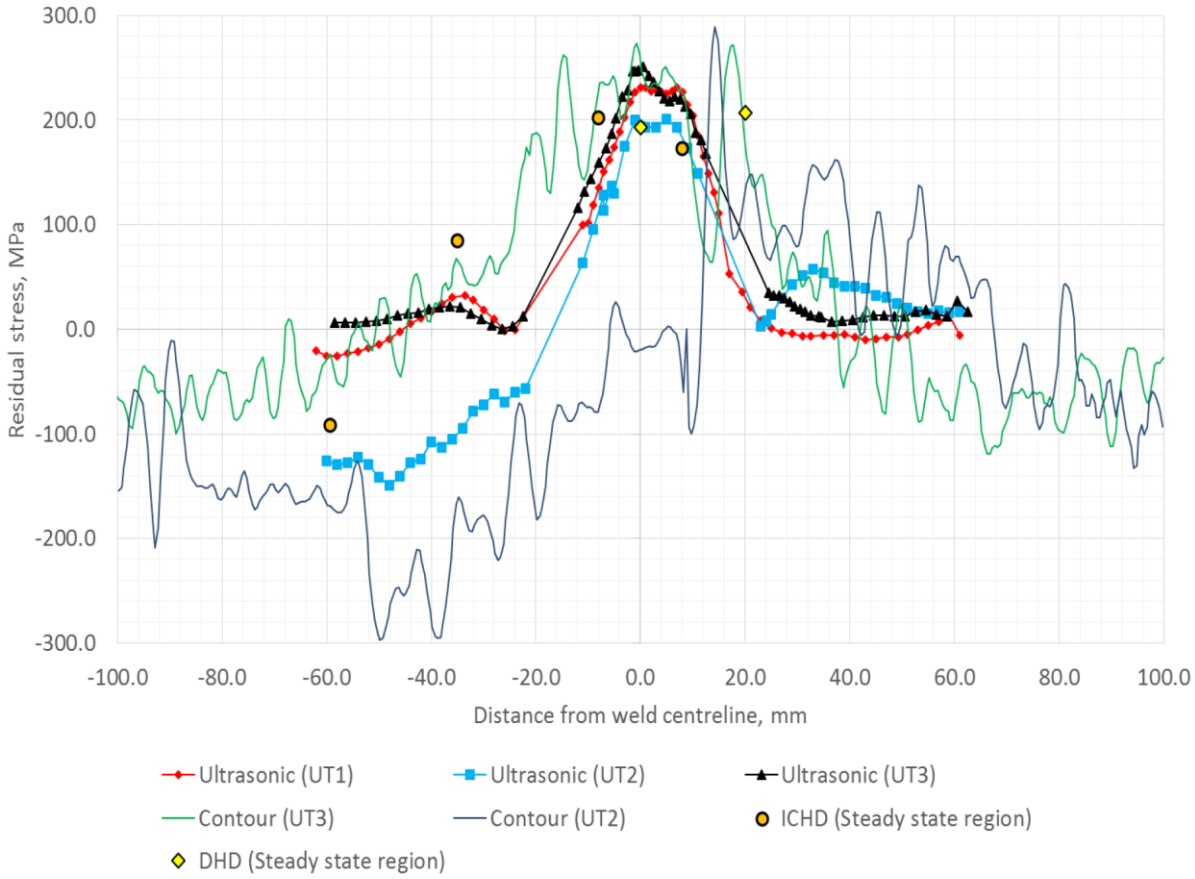

Figure 44: Comparison of ultrasonic measurements to those obtained through contour measurements and hole drilling measurements. In the figure UT1 corresponds to a section done across a circumferential weld, UT2 corresponds to a section done across the intersection of the longitudinal and circumferential welds, and UT3 corresponds to a section across a longitudinal weld.

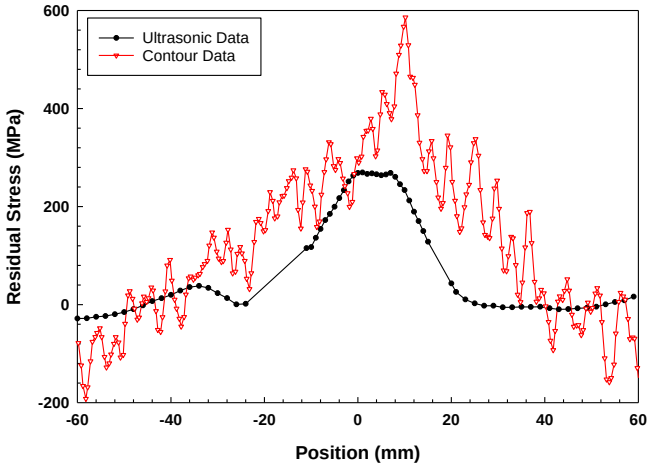

Figure 45: Comparison of the ultrasonic measurement data and un-averaged contour measurement data for the circumferential weld. Note that the peak stresses are lost in the ultrasonic measurement.

6. FUTURE CHARACTERIZATION ACTIVITIES

This report documents the results of residual stress measurements on the full-diameter canister mockup. Other characterization activities are ongoing, and will be documented in future reports.

6.1 Weld Metallurgical Condition and Degree of Sensitization

Assessment of the microstructure of the regions at the longitudinal, circumferential, and repair welds will be performed using standard metallurgical techniques. An effort will be made to perform these analyses in the same basic regions as the residual stress measurements such that the two can be correlated.

The thermal cycling associated with the welding process, in addition to altering the overall microstructure of the near-weld material, can result in the precipitation of chromium-rich carbides and the concomitant formation of chromium depleted regions along the grain boundaries. This effect, known as sensitization, will be particularly pronounced in the weld HAZ (i.e., material in a region near the weld FZ that is heated to peak temperatures up to the effective solidus). The extent to which sensitization has taken place will be documented as a function of position from the edge of the weld FZ. This will be done both for the near surface regions, as well as through the thickness of the container wall. A volumetric assessment of the degree of sensitization will illustrate the extent of the region and illustrate the presence/absence of an active path for crack propagation through the material.

Samples taken from the container will be prepared metallographically and evaluated electrochemically for the degree of sensitization. Evaluation will be done through either the single loop electrochemical reactivation (EPR) test or double-loop EPR test. For the single loop test, as defined in ASTM International (ASTM) specification G108 "Standard Test Method for Electrochemical Reactivation (EPR) for Detecting Sensitization of AISI Type 304 and 304L Stainless Steels" (ASTM, 2010), the surface to be analyzed is polarized anodically such that the surface is activated. This results in enhanced dissolution of the chromium depleted grain boundaries, while the remainder of the grain is rendered passive. The net charge associated with dissolution of the chromium depleted regions along the grain boundaries is determined based upon the total current passed during the aforementioned polarization. This technique requires characterizing the microstructure of the material (specifically, the grain size), such that the overall charge per unit area of grain boundary can be calculated, the magnitude of which defines the extent of sensitization. The second technique is a modification of the first, and is more suitable for instances where the surface finish of the material being evaluated is less well defined, or measurement of the grain size within the material is difficult. This technique, described in Scully (1995), is known as the double-loop EPR technique. In this method, the sample is essentially subjected to the same polarization as the single loop EPR, but it is applied twice. The ratio of the peak currents extracted from the first and second polarization is then recorded. The magnitude of this ratio is directly related to the degree of sensitization of the material. For an un-sensitized microstructure, the first polarization passivates the sample, such that the peak current from the second polarization is considerably lower than the first. However, in the case of a sensitized microstructure, the chromium depleted zones are not passivated by the first polarization, and the peak current for the second polarization will be large, approaching the value of the first polarization. The magnitude of the ratio is used to assess the degree of sensitization, with the value approaching 1 for heavily sensitized materials.

In the event that the electrochemical techniques are insufficient to define the degree of sensitization of the container wall material, alternate methods will be pursued, such as those defined in ASTM A262 "*Standard Practices for Detecting Susceptibility to Intergranular Attack in Austenitic Stainless Steels"* (ASTM, 2014). This specification provides a series of immersion tests designed to activate grain boundaries such that the extent of attack can be assessed either via metallography or weight change measurement.

Positional mapping of the degree of sensitization will be accomplished by selectively mapping regions of the surface using plating tape or a similar material. The exposed region will be selected such that a

sufficient number of grains are evaluated in each test. Replicate measurements will be accomplished by grinding the surface upon the completion of each successive set of experiments, such that the region immediately below the first set of measurements can be performed. This procedure will be repeated for each of the regions where the stress distribution is assessed (i.e., the circumferential, longitudinal, and repair welds).

6.2 Stress Corrosion Cracking Susceptibility

Establishing the susceptibility to SCC will require both the resistance to crack nucleation as well as the magnitude of crack propagation to be assessed as a function of the environmental conditions to which the container is subjected while exposed to stresses as defined by the full scale mockup. A wide variety of experiments are planned,

1. The information learned from the residual stress measurements, combined with the electrochemically determined degree of sensitization will enable the fabrication of material simulating the weld HAZ. The samples will be subjected to the same thermomechanical processing to which the HAZ has been subjected using a Gleeble, a simulator capable of replicating the thermal and mechanical history of the HAZ. These samples will then be used in simple U-bend experiments, where marine aerosols are deposited on the surface of the bent portion of the sample (replicating the surface deposits observed via in-service inspections, as well as predicted worst-case deposits), then subjected to combinations of humidity and temperature typical of coastal ISFSI sites. These experiments will be used to evaluate SCC initiation under relevant conditions and with relevant materials and stresses.
2. Crack propagation studies will be conducted using compact tension specimens where the microstructure has been modified so as to accurately simulate the condition in the HAZ of actual storage containers, and tensile stresses will cover the range of residual stresses measured in the mockup welds. The surface deposits and exposure conditions will be similar to those explored for U-bend specimens.

Specimens taken from the large scale mockup, sized so as to maintain a residual stress distribution similar to that for the as-received condition, will be used for crack initiation and propagation studies. A combination of worst case and field representative deposits will be placed on the surface of the samples, after which they will be exposed to relevant temperature and humidity conditions. It should be noted that mockup samples will be relatively large and limited in number, so the aforementioned tests will be used to define the conditions used to evaluate specimens taken from the mockup.

7. WELD SAMPLE DISSEMINATION TO INTERESTED PARTIES

The mockup weld samples, in addition to being critical for the UFD program, are also of great interest to outside parties such as EPRI and academic groups working on storage-related NEUP programs. Meetings will be held with each of the interested parties to assess their needs. Utilizing the information from each party, a larger prioritized list of coupons will be assembled. The needs of the UFD program will be given first priority, followed by the DOE funded NEUP groups and EPRI.

8. CONCLUSIONS

The purpose of the work reported in this document was to establish the residual stress state associated with weldments in a typical welded stainless steel interim storage container. A mock-up container was produced utilizing dual-certified 304/304L SS welded with 308L SS, replicating a NUHOMS 24P dry storage cask using the same protocols and procedures used to fabricate the containers at the Calvert Cliffs nuclear power station. Once fabricated, an array of techniques was used to characterize the container residual stresses at base metal locations far from the welds, at circumferential and longitudinal welds, at a weld intersection, and finally, at a simulated weld repair. Both iDHD and the Contour Method techniques were able to document the stress state through the thickness of the container wall. The results using these two techniques were generally consistent; relatively minor observed variations were likely due to relaxation due to cutting prior to applying the Contour Method. For both circumferential and longitudinal welds, large tensile stresses, well in excess of the uniaxial yield strength, were found through the entire container wall, both in the weld FZ as well as the weld HAZ. Even higher tensile stresses were measured around a simulated weld repair zone on one of the circumferential welds. Elevated tensile stresses extended outwards to a distance of ~40 mm from the weld centerline for circumferential welds and 25mm from the weld centerline for longitudinal welds. Analyses performed in the base metal indicated that while stresses close to the outer diameter were tensile in nature, they became compressive midway through the wall, consistent with the anticipated stress distribution for a bent plate.

To summarize:

- An interim storage container mockup was produced using standard methodologies applied by most manufacturers of existing, fielded storage systems
- The residual stress distributions associated with all of the welds used to fabricate the mockup were measured
- Stress distributions for the base metal became compressive at mid thickness, suggesting a crack which initiates in such regions would not have sufficient driving force to progress through wall
- Stress distributions were strongly tensile completely through the container wall at weldments
    - Highest stresses were parallel to the direction in which the weld was made
    - Suggest tensile driving force exists to support through wall crack propagation (note – stress is a necessary, but not sufficient, condition for SCC crack propagation)
- An assessment of an ultrasonic residual stress measurement method revealed that it is effective, with the potential to offer a precision comparable to other techniques that, while they yield a more complete map (e.g., contour measurement or deep hole drilling), are destructive in nature and as such may not be used in many applications.

9. REFERENCES

ASTM. (2010). Method G108-94 (2010): Standard Test Method for Electrochemical Reactivation (EPR) for Detecting Sensitization of AISI Type 304 and 304L Stainless Steels. West Conshohocken, PA: ASTM International.

ASTM. (2014). Method A262-14: Standard Practices for Detecting Susceptibility to Intergranular Attack in Austenitic Stainless Steels. West Conshohocken, PA: ASTM International.

Bouchard, P., George, D., Santisteban, J., Bruno, G., Dutta, M., Edwards, L., Kingston, E. and Smith, D. (2005). Measurement of the residual stresses in a stainless steel pipe girth weld containing long and short repairs. International Journal of Pressure Vessels and Piping 82, 299-310.

Benson, M., Rudland, D. J. & Csontos, A. (2014). Weld Residual Stress Finite Element Analysis Validation: Part 1, Data Development Effort. U.S. NRC.

Bryan, C. R. and Enos, D. (2014). Analysis of Dust Samples Collected from Spent Nuclear Fuel Interim Storage Containers at Hope Creek, Delaware, and Diablo Canyon, California, SAND2014-16383. Albuquerque, NM. Sandia National Laboratories.

Bryan, C. R. and Enos, D. G. (2015). Analysis of Dust Samples Collected from an Unused Spent Nuclear Fuel Interim Storage Container at Hope Creek, Delaware, SAND2015-1746. Albuquerque, NM. Sandia National Laboratories.

Cook, A., Stevens, N., Duff, J., Mishelia, A., Leung, T. S., Lyon, S., Marrow, J., Ganther, W. and Cole, I. (2011). Atmospheric-induced stress corrosion cracking of austenitic stainless steels under limited chloride supply. Proc. 18th Int. Corros. Cong., Perth, Australia.

Cook, A., Lyon, S., Stevens, N., Gunther, M., McFiggans, G., Newman, R. and Engelberg, D. (2014). Assesing the Risk of Under-Deposit Chloride-Induced Stress Corrosion Cracking in Austenitic Stainless Steel Nuclear Waste Containers. Corrosion Engineering, Science and Technology 49, 529-534.

Dong, P., Zhang, J. and Bouchard, P. (2002). Effects of repair weld length on residual stress distribution. Journal of pressure vessel technology 124, 74-80.

Dong, P., Hong, J. and Bouchard, P. (2005). Analysis of residual stresses at weld repairs. International Journal of Pressure Vessels and Piping 82, 258-269.

Elcoate, C., Dennis, R., Bouchard, P. and Smith, M. (2005). Three dimensional multi-pass repair weld simulations. International Journal of Pressure Vessels and Piping 82, 244-257.

Enos, D. G., Bryan, C. R. and Norman, K. M. (2013). Data Report on Corrosion Testing of Stainless Steel SNF Storage Canisters, FCRD-UFD-2013-000324. U.S. Department of Energy, Office of Used Nuclear Fuel Disposition.

Enos, D. & Bryan, C. (2014). Technical Work Plan: Characterization of Weld Regions on a Full-Scale Cylindrical Mockup of an Interim Storage Container. Albuquerque, NM: U.S. Department of Energy, 17.

EPRI. (2011). Extended Storage Collaboration Program (ESCP) Progress Report and Review of Gap Analyses. Palo Alto, CA.

EPRI. (2014). Calvert Cliffs Stainless Steel Dry Storage Canister Inspection. Palo Alto, CA.

Gellrich, G. H. (2013). Response to Request for Additional Information, Re: Calvert Cliffs Independent Spent Fuel Storage Installation License Renewal Application (TAC No. L24475) dated April 24, 2013, NRC Adams accession numbers ML13119A242, ML13119A243, and ML13119A244.

George, D. and Smith, D. (2005). Through thickness measurement of residual stresses in a stainless steel cylinder containing shallow and deep weld repairs. International Journal of Pressure Vessels and Piping 82, 279-287.

Ghosh, S., V. Kain (2010) "Effect of Surface Machining and Cold Working on the Ambient Temperature Chloride Stress Corrosion Cracking Susceptibility of AISI 304L Stainless Steel", Materials Science and Engineering A, 527, pp. 679-683.

Hanson, B., Alsaed, H., Stockman, C., Enos, D., Meyer, R. and Sorenson, K. (2012). Gap analysis to support extended storage of used nuclear fuel, FCRD-USED-2011-000136. U.S. Department of Energy.

Hayashibara, H., Mayuzumi, M. and Mizutani, Y. (2008). Effects of temperature and humidity on atmospheric stress corrosion cracking of 304 stainless steel. CORROSION 2008.

Hossain, S., Truman, C., Smith, D. and Bouchard, P. (2006). Measurement of residual stresses in a type 316H stainless steel offset repair in a pipe girth weld. Journal of pressure vessel technology 128, 420-426.

Hossain, M., Goudar, D., Truman, C. E. and Smith, D. J. (2011). Simulation and measurement of residual stresses in a type 316h stainless steel offset repair in a pipe girth weld. Materials Science Forum: Trans Tech Publ, 492-497.

Kain, R. M. (1990). Marine atmosphere corrosion cracking of austenitic stainless steels. Materials Performance 29, 60-62.

Kosaki, A. (2008). Evaluation method of corrosion lifetime of conventional stainless steel canister under oceanic air environment. Nuclear Engineering and Design 238, 1233-1240.

Mahmoudi, A., Hossain, S., Truman, C., Smith, D. and Pavier, M. (2009). A new procedure to measure near yield residual stresses using the deep hole drilling technique. Experimental Mechanics 49, 595-604.

Mahmoudi, A., Truman, C., Smith, D. and Pavier, M. (2011). The effect of plasticity on the ability of the deep hole drilling technique to measure axisymmetric residual stress. International Journal of Mechanical Sciences 53, 978-988.

Mintz, T. S., Caseres, L., He, X., Dante, J., Oberson, G., Dunn, D. S. and Ahn, T. (2012). Atmospheric Salt Fog Testing to Evaluate Chloride-Induced Stress Corrosion Cracking of Type 304 Stainless Steel. Corrosion 2012. Salt Lake City, March 11-15: NACE.

Nakayama, G. (2006). Atmospheric stress corrosion cracking (ASCC) susceptibility of stainless alloys for metallic containers. In: VanIseghem, P. (ed.) Scientific Basis for Nuclear Waste Management XXIX, pp. 845-852.

Nakayama, G. and Sakakibara, Y. (2013). Prediction Model for Atmospheric Stress Corrosion Cracking of Stainless Steel. ECS Transactions 50, 303-311.

NWTRB. (2010). Evaluation of the technical basis for extended dry storage and transportation of used nuclear fuel. Arlington, VA. Nuclear Waste Technical Review Board.

NRC. (2012a). Identification and Prioritization of the Technical Information Needs Affecting Potential Regulation of Extended Storage and Transportation of Spent Nuclear Fuel. Draft for comment. Washington, D.C. U.S. NRC.

NRC. (2012b). Potential Chloride Induced Stress Corrosion Cracking of Austenitic Stainless Steel and Maintenance of Dry Cask Storage System Canisters. Washington, D.C.: U.S. NRC.

NRC. (2013). Finite Element Analysis of Weld Residual Stresses in Austenitic Stainless Steel Dry Cask Storage System Canisters, NRC Technical Letter Report (ADAMS ML13330A512). Washington D.C. Nuclear Regulatory Commission.

Pacific Nuclear Fuel Services, I. (1991). Topical Report for the NUTECH Horizontal Modular Storage System for Irradiated Nuclear Fuel NUHOMS-24P, Document NUH-002 Rev. 2A, April 1991. Adams ML110730769

Parrott, R. and Pitts, H. (2011). Chloride stress corrosion cracking in austenitic stainless steel: Assessing susceptibility and structural integrity. U.K. Health and Safety Executive

Prosek, T., Iversen, A. and Taxén, C. (2009). Low temperature stress corrosion cracking of stainless steels in the atmosphere in presence of chloride deposits. Corrosion 65, 105-117.

Prosek, T., Le Gac, A., Thierry, D., Le Manchet, S., Lojewski, C., Fanica, A., Johansson, E., Canderyd, C., Dupoiron, F. and Snauwaert, T. (2014). Low temperature stress corrosion cracking of austenitic and duplex stainless steels under chloride deposits. Corrosion.

Scully, J. R. (1995). Electrochemical Tests. In: Baboian, R. (ed.) Corrosion Tests and Standards: Application and Interpretation. ASTM manual series, MNL-20. West Conshohocken, PA: ASTM International.

Tani, J. I., Mayuzurmi, M. and Hara, N. (2009). Initiation and propagation of stress corrosion cracking of stainless steel canister for concrete cask storage of spent nuclear fuel. Corrosion 65, 187-194.